Microfluid Nanofluid (2011) 10:1–28
DOI 10.1007/s10404-010-0624-1

REVIEW

Lattice Boltzmann method for microfluidics: models and applications

Junfeng Zhang

Received: 29 January 2010 / Accepted: 12 April 2010 / Published online: 28 April 2010

Abstract The lattice Boltzmann method (LBM) has experienced tremendous advances and has been well accepted as a useful method to simulate various fluid behaviors. For computational microfluidics, LBM may present some advantages, including the physical representation of microscopic interactions, the uniform algorithm for multiphase flows, and the easiness in dealing with complex boundary. In addition, LBM-like algorithms have been developed to solve microfluidics-related processes and phenomena, such as heat transfer, electric/magnetic field, and diffusion. This article provides a practical overview of these LBM models and implementation details for external force, initial condition, and boundary condition. Moreover, recent LBM applications in various microfluidic situations have been reviewed, including microscopic gaseous flows, surface wettability and solid–liquid interfacial slip, multiphase flows in microchannels, electrokinetic flows, interface deformation in electric/magnetic field, flows through porous structures, and biological microflows. These simulations show some examples of the capability and efficiency of LBM in computational microfluidics.

Keywords Lattice Boltzmann method · Microfluidics · Interfacial phenomena · Multiphase flows · Bubble/droplet dynamics · Electrokinetics · Interfacial slip · Numerical simulation

J. Zhang (✉)
School of Engineering, Laurentian University, 935 Ramsey Lake Road, Sudbury, ON P3E 2C6, Canada
e-mail: jzhang@laurentian.ca

1 Introduction

Microfluidics studies the behaviors of small volume of fluids, typically in the order of microliters, nanoliters, or even picoliters. The fluid dimensions in microfluidic systems range from millimeters down to micrometers. Applications involving microfluidics cover a wide spectrum, including micro-electro-mechanical systems (MEMS) (Beskok et al. 1996; Gad-el-Hak 1999), fuel cells (de Jong et al. 2006), oil recovery (Upreti et al. 2007), chemical and biology analysis (Li 2004), and biomedical devices (Nisar et al. 2008; Haber 2006). With recent technical advances, experimental investigations of some fluid behaviors in microfluidic systems are possible and are becoming more accessible. However, theoretical and numerical analyses are still usually necessary to reveal underlying mechanisms, to examine the various effects involved, to provide design guidelines for practical applications, and even to interpret experimental observed phenomena. Theoretical analysis is certainly limited to very simple situations, and therefore, most often, numerical simulations are employed to obtained detailed, in-depth information, especially for that which is not available from direct experiments.

Depending on the fluid states, flows in microfluidic systems could be gaseous (also referred as microflows)-, liquid-, or multiphase-flows. For microscopic gaseous flows, due to the rarefaction effects and lack of local equilibrium, traditional continuum assumption of a homogeneous fluid is no longer appropriate (Gad-el-Hak 1999; Tang et al. 2008). Particular flow features, such as velocity slip and temperature jump over solid boundaries, have been noticed in experiments. The Knudsen number $K_n = \lambda/L$, the ratio of the gas mean free path λ to a characteristic length of the flow domain L, usually serves as a criterion in determining whether the continuum assumption is

applicable to a fluid flow. On the other hand, for microscopic liquid and multiphase flows, although the fluid can be still described as a continuum substance, due to the high surface-area-to-volume ratio, microscopic interactions and related interfacial phenomena, such as electrokinetics, surface wettability, and interfacial slip, which are typically neglected in macroscopic systems, have to be considered carefully (Li 2004; Fair 2007; Gad-el-Hak 1999; Madou et al. 2006).

Traditional computational fluid dynamics (CFD) methods start from the continuum equations and solve them numerically by appropriate schemes. However, such an approach has difficulties to incorporate the microscopic interactions, which are crucial in many microfluidic circumstances, for example, the dynamics of wetting and interfacial slip. On the other hand, microscopic simulation approach, such as molecular dynamics (MD), studies the fluid behaviors by the evolution of individual molecules interacting with each other through intermolecular potentials. Here the microscopic molecular structures and interactions are well represented; however, the huge computation demand limits its applications to very small space and time scales, even with the most advanced supercomputers (Kadau et al. 2006).

Between the macroscopic and microscopic approaches, there exist several mesoscopic methods, such as the dissipative particle dynamics (DPD) (Besold et al. 2000) and the lattice Boltzmann method (LBM) (Succi 2001; Chen and Doolen 1998; Sukop and Thorne 2006), as representatives. DPD is a mesh-free particle-based method for fluids and other soft matters and can be considered as a coarse-grained version of MD. A particle in DPD represents a collection of molecules and such particles are interacting with each other via conservative, dissipative, and random forces. However, the algorithm involves a group of parameters, and their quantities are not directly related to interested macroscopic parameters (Filipovic et al. 2009).

LBM has experienced rapid development and attracted increasing interests during the past two decades in simulating complex fluid systems and other processes and phenomena. LBM models the fluid as fictitious particles, and such particles perform consecutive propagation and collision processes over a discrete lattice mesh. Due to its particulate nature and local dynamics, LBM has several advantages over conventional CFD methods. For example, mesh refinement or boundary-fitted grid is usually necessary for arbitrary boundaries in CFD simulations (Tu et al. 2007). However, LBM can relatively easily implement such complex boundaries by imposing, for example, the bounce-back or modified bounce-back schemes (see Sect. 2.4.1) to the fluid particle distributions, as demonstrated in simulations of porous flows (Martys and Chen 1996; Koido et al. 2008) and particulate suspension flows (Ladd 1994a; Heemels et al. 2000; Joshi and Sun 2009). LBM also exhibits some attractiveness for incorporating microscopic interactions and implementing parallel computation (Succi 2001). In addition, the pressure field is also directly available from the density distribution; hence efforts to obtain the pressure field by, for example, solving a Poisson equation in the so-called projection method (Tu et al. 2007) can be saved in LBM.

Historically, LBM originated from the lattice gas automata (LGA), which can be considered as a simplified, fictitious version of MD in which space, time, and particle velocities are all discrete. Each lattice node is connected to its neighbors by, for example, six lattice velocities in a hexagonal FHP model (Succi 2001, Sukop and Thorne 2006). There can be either one or none particle at a lattice node moving along a lattice direction. After a time interval, each particle then moves to the neighboring node in its direction, and this process is called propagation. When there are more than one particles arriving at the same node from different directions, they collide and change their directions according to a set of collision rules. Good collision rules should conserve the particle number (mass), momentum, and energy before and after the collision. In spite of its many successful applications, LGA suffers from several native defects including the lack of Galilean invariance, presence of statistical noise and exponential complexity for three-dimensional lattices (Succi 2001).

The main motivation for the transition from LGA to LBM was the desire to remove statistical noise by replacing the Boolean particle number in a lattice direction with its ensemble average, the so-called density distribution function. Accompanying with this replacement, the discrete collision rules also have to be modified as a continuous function—the collision operator. It has been also shown that the LBM scheme can be interpreted as a special discretized form of the continuous Boltzmann equation (Sterling and Chen 1996; He and Luo 1997; Abe 1997). Through a Chapman–Enskog analysis, one can recover the governing continuity and Navier–Stokes equations from the LBM algorithm (Buick 1997).

Simulating multiphase/multicomponent flows have always been a challenge because of the moving and deformable interfaces. Physically, interfaces between two bulk fluid phases (e.g., liquid and vapor) originate from the specific interactions among molecules. In LBM, the particle kinetics allows a relatively easy and consistent avenue to incorporate the underlying microscopic interactions. Several LBM multiphase/multicomponent models have been developed. Phase separations can be generated automatically from particle dynamics and no special treatment is needed to manipulate the interfaces as in some traditional CFD methods, such as the volume of fluid (VOF)

and level set methods. Successful applications of the multiphase/multicomponent LBM models can be found in various complex fluid systems, including interface instability, bubble/droplet dynamics, wetting on solid surfaces, interfacial slip, capillary filling, and electrohydrodynamic and magnetohydrodynamic interface deformations.

From a pure computational point of view, the general LBM can be considered as a numerical solver of macroscopic momentum conservation equation, i.e., the Navier–Stokes equation, which is a nonlinear, second-order partial differential equation. For this reason, several LBM-like algorithms have also been proposed to solve various differential equations governing other physical processes and phenomena, such as heat transfer, electric field, magnetic field, diffusion processes, flows in porous materials, and shallow flows. Such models inherit the advantages in programming and parallel computation, but have no physics involved.

Several excellent reviews and books on LBM (Benzi et al. 1992; Chen and Doolen 1998; Raabe 2004; Succi 2001; Sukop and Thorne 2006; Wolf-Gladrow 2000; Aidun and Clausen 2010; Wang and Pan 2008; Dunweg and Ladd 2009) have been published. However, the particular applications and strengths of LBM in simulating microfluidic behaviors have not been well addressed. In this review, we describe the basic LBM algorithms and typical simulation techniques for general fluid dynamics. We also introduce LBM models for other processes and phenomena, which may be useful in microfluidics, such as multiphase/multicomponent flows, diffusion-convection, heat transfer, electrical field, and magnetic field. Moreover, representative LBM simulations will be reviewed to demonstrate its usefulness in computational microfluidics.

2 LBM for fluid dynamics

2.1 The lattice Bhathagar–Gross–Krook Boltzmann model

LBM can be considered as a particular discrete version of the Boltzmann theory with time, space, and momentum all discretized (He and Luo 1997; Abe 1997). In LBM, a fluid is modeled as fictitious particles moving with several lattice velocity (momentum discretization) in a lattice domain (space discretization) at consequential time steps (time discretization). Typical D2Q9 (two-dimensional and nine-velocity) square and D3Q19 (three-dimensional and 19-velocity) cube lattice structures, which are commonly utilized in LBM simulations among many other options (Wolf-Gladrow 2000), are shown in Fig. 1. For simplicity, here we take the D2Q9 model as an example for our discussion. Details for other models are similar and readily available in the literature.

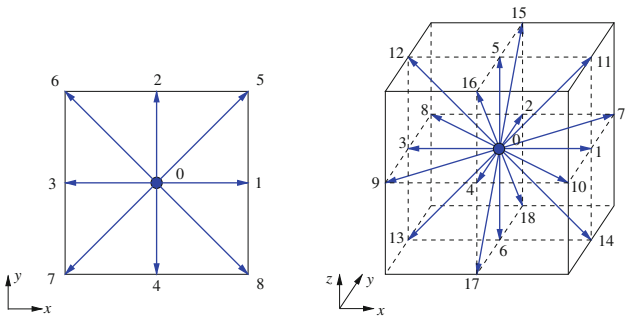

Fig. 1 Schematics of the D2Q9 (*left*) and D3Q19 (*right*) lattice models. The edge length of both the D2Q9 square and the D3Q19 cube is $2\Delta x/\Delta t$, and *dashed lines* show the midplanes of the D3Q19 cube. The lattice velocities are indicated by *arrows* starting from the square/cube center. Note there is a zero lattice velocity $\mathbf{c}_0 = \mathbf{0}$ in both the models

The nine lattice velocities of the D2Q9 model are

$$\begin{aligned} \mathbf{c}_0 &= \mathbf{0}, \\ \mathbf{c}_i &= \left(\cos\frac{i-1}{2}\pi,\ \sin\frac{i-1}{2}\pi\right)\frac{\Delta x}{\Delta t}, \quad i = 1{-}4, \\ \mathbf{c}_i &= \sqrt{2}\left(\cos\frac{2i-9}{4}\pi, \sin\frac{2i-9}{4}\pi\right)\frac{\Delta x}{\Delta t}, \quad i = 5{-}8, \end{aligned} \tag{1}$$

where Δx and Δt are, respectively, the lattice unit and the time step. The major variable in LBM is the density distribution $f_i(\mathbf{x}, t)$, indicating the portion of particles moving with the ith lattice velocity at lattice site $\mathbf{x}$ and time t. Since $\mathbf{c}_0 = (0, 0)$, f_0 corresponds to the portion that does not move at all. After one time step Δt, $f_i(\mathbf{x}, t)$ will arrive at its neighboring lattice site $\mathbf{x} + \mathbf{c}_i\Delta t$ along the lattice velocity $\mathbf{c}_i$. This process is usually called the streaming or propagation process. Since there are other particles coming to this same site from different directions, collision among them will occur at this site, and the original particle numbers moving in each direction will be changed. After this collision, a new set of density distributions leaves the collision site in different lattice velocities, and another propagation process starts. In a LBM simulation, such propagation and collision processes are repeated again and again till satisfied results are achieved.

The above-mentioned dynamics can be expressed by the so-called lattice Boltzmann equation (LBE)

$$f_i(\mathbf{x} + \mathbf{c}_i\Delta t, t + \Delta t) - f_i(\mathbf{x}, t) = \Omega_i(f). \tag{2}$$

Here, Ω_i is the collision operator, which takes account of the distribution change after a collision. The left-hand side represents the propagation process as discussed above. In the LBM development, an important simplification is to approximate the collision operator with the Bhathagar–Gross–Krook (BGK) single relaxation time approximation,

which was originally proposed for Boltzmann equation in continuum kinetic theory (Bhatnagar et al. 1954). The lattice BGK (LBGK) equation can then be written as:

$$f_i(\mathbf{x}+\mathbf{c}_i\Delta t, t+\Delta t) - f_i(\mathbf{x},t) = -\frac{f_i(\mathbf{x},t) - f_i^{\mathrm{eq}}(\mathbf{x},t)}{\tau}, \quad (3)$$

where τ is a relaxation parameter toward the equilibrium distribution f_i^{eq}, which can be expressed as a discretization of the Maxwell–Boltzmann equilibrium distribution (Qian et al. 1992):

$$f_i^{\mathrm{eq}} = \rho w_i \left[1 + \frac{\mathbf{u}\cdot\mathbf{c}_i}{c_s^2} + \frac{1}{2}\left(\frac{\mathbf{u}\cdot\mathbf{c}_i}{c_s^2}\right)^2 - \frac{\mathbf{u}\cdot\mathbf{u}}{2c_s^2}\right], \quad (4)$$

Here, the fluid density ρ and velocity $\mathbf{u}$ can be readily obtained from the density distributions at each lattice site through

$$\rho = \sum_i f_i, \quad \rho\mathbf{u} = \sum_i f_i \mathbf{c}_i. \quad (5)$$

Other parameters, including the lattice sound speed c_s and weight factor w_i, are lattice structure-dependent. For our D2Q9 model here $w_0 = 4/9$, $w_{1-4} = 1/9$, $w_{5-8} = 1/36$, and $c_s^2 = \Delta x^2/3\Delta t^2$. Through the Chapman–Enskog expansion, one can recover the macroscopic continuity and momentum (Navier–Stokes) equations from the above-defined LBM dynamics (Buick 1997):

$$\begin{aligned} &\frac{\partial\rho}{\partial t} + \nabla\cdot(\rho\mathbf{u}) = 0, \\ &\frac{\partial\mathbf{u}}{\partial t} + (\mathbf{u}\cdot\nabla)\mathbf{u} = -\frac{1}{\rho}\nabla p + \nu\nabla^2\mathbf{u}, \end{aligned} \quad (6)$$

with the kinematic shear viscosity ν given by

$$\nu = \left(\tau - \frac{1}{2}\right)c_s^2\Delta t. \quad (7)$$

and the pressure P expressed as

$$P = c_s^2\rho. \quad (8)$$

For incompressible microscopic flows, the Mach number $Ma = U/c_s$ (U is a characteristic flow velocity) should be low in LBM simulations.

There are several other more complicated LBM schemes proposed for fluid dynamics. For example, a multiple relaxation times (MRT) model can improve the numerical stability and offers the option of adjusting the bulk and shear viscosities independently (d'Humieres et al. 2002; Lallemand and Luo 2000). On the other hand, carefully designed off-grid lattice structures have been developed for microscopic flows at finite Knudsen numbers (Shan et al. 2006; Zhang et al. 2006). Unstructured LBM is also available for complex geometry boundaries (Ubertini and Succi 2005).

It can be seen from the above description that the LBM dynamics is local (i.e., only the very neighboring lattice nodes are involved in updating the density distributions), and hence LBM algorithm is advantageous for parallel computations. Moreover, the pressure field is directly available from the distribution functions via Eq. 8, and therefore the effort to compute the pressure field has been saved when compared with some other CFD methods (e.g., solving a Poisson equation in the projection method). Comparisons of computational efficiency between LBM and other CFD methods have also been reported. For example, Wang et al. (2007a) have compared a LBM algorithm for fluid–solid conjugate heat transfer to a commercial CFD software. Their simulations indicated that the classical CFD method needs much finer mesh than the LBM model to obtain a same accuracy, and the CFD computational time was over twice of that for LBM even for a simple geometry. It is anticipated that such computational advantage would be more significant in actual complex geometries. Yoshino et al. (2004) have also confirmed that LBM is more efficient that the finite difference method in simulating flows through porous materials, because of the LBM strength in dealing with complex boundaries and also the computational saving in not solving pressure field. However, opposite observations have also been reported for flows in simple geometry (Lai et al. 2001; Al-Zoubi and Brenner 2004; Geller et al. 2006). It should be noted that tremendous efforts have been devoted on optimizing the efficiency of classical CFD methods, while most LBM studies still focus on model development and scientific applications in various situations. Actually some studies have indeed shown that the LBM simulation efficiency could be dramatically improved by utilizing various computational techniques, such as adaptive hierarchical grids, particular data structures, memory management, and parallelization strategies (Schulz et al. 2002; Toolke et al. 2006; Freudiger et al. 2008). In addition, in recent years, the graphics processing units (GPUs), which are originally developed for computer games, have provided an inexpensive but very efficient alternative to LBM simulations (Tolke and Krafczyk 2008; Kaufman et al. 2009; Kuznik et al. 2010). Therefore, it is reasonable to anticipate that in the near future LBM simulations would be generally accepted as an efficient choice for suitable situations.

2.2 Force implementation in LBM

Many microfluidic systems involve external or internal forces, such as gravity (Kang et al. 2002; Yamaguchi et al. 2007), electric or magnetic force (Li 2004; Qian and Bau 2009), centrifugal force (Zhang et al. 2009c), and fluid–particle interactions (Kang and Li 2009; Zhang et al.

2009a). Physically, the effect of a body force can be interpreted as an injection of momentum into the fluid. Therefore, to incorporate the forcing effect on fluid motion, the LBE is typically modified by adding a forcing term after the collision (He et al. 1997), which can be considered as the counterpart of the forcing term in the original Boltzmann equation in the kinetic theory:

$$f_i(\mathbf{x}+\mathbf{c}_i\Delta t, t+\Delta t) - f_i(\mathbf{x},t) = -\frac{f_i(\mathbf{x},t) - f_i^{\mathrm{eq}}(\mathbf{x},t)}{\tau} + \frac{w_i \Delta t}{c_s^2}\mathbf{F}\cdot\mathbf{c}_i, \tag{9}$$

where $\mathbf{F}$ is the body force applied to the fluid of a unit volume. Alternatively, an equilibrium velocity can be introduced for the purpose of calculating equilibrium distributions f_i^{eq} in Eq. 4 as (Shan and Chen 1993):

$$\mathbf{u}^{\mathrm{eq}} = \frac{1}{\rho}\left(\sum_i f_i\mathbf{c}_i + \tau\Delta t\mathbf{F}\right). \tag{10}$$

It can be shown that these modifications increase the fluid momentum at a lattice node by an amount of $\Delta t\mathbf{F}$ during each time step without changing the fluid density. The Navier–Stokes equation resulting from the Chapman–Enskog analysis has the correct body force term added to the right-hand side. Several other schemes have also been utilized in LBM simulations (He et al. 1998; Wang et al. 2006; Ladd and Verberg 2001; Buick and Greated 2000; Guo et al. 2002a).

2.3 Initial condition

The principal variable in a LBM simulation is the distribution function f_i, which is updated at each time step according to the LBE. To start such a simulation, some initial values must be assigned to these distribution functions in each lattice direction at each fluid node. Typically, we adopt the equilibrium distribution functions calculated from Eq. 4 with initial velocity $\mathbf{u}_0 = \mathbf{u}(\mathbf{x}, t = 0)$ and an assumed constant density $\rho(\mathbf{x}, t = 0) = \rho_0$, i.e.,

$$f_i(\mathbf{x}, t=0) = f_i^{\mathrm{eq}}(\mathbf{x}, t=0) = f_i^{\mathrm{eq}}(\rho_0, \mathbf{u}_0). \tag{11}$$

Usually ρ_0 is set to unity for simplicity. Note such an assumption of $f_i \approx f_i^{\mathrm{eq}}$ will be exactly valid, as observed in Eq. 2, if only when $\tau = 1$ or when the fluid density and velocity are both uniform and steady over the entire domain. Such constraints are generally not satisfied and, therefore, cautions should be executed when interpreting the simulation results of the beginning period. Fortunately, in most situations, we are investigating the steady or well-developed flow behaviors and the initial condition effect will not be a major concern. For the transient process followed a particular initial flow field, more delicate treatments can be considered (Skordos 1993; Mei et al. 2006).

2.4 Boundary conditions

As with other numerical approaches, appropriate boundary conditions are crucial for meaningful simulations. For a lattice node near a boundary, density distributions entering the fluid domain after the propagation step are not available. The boundary conditions must then be implemented by specifying the unknown f_i entering the simulation domain across boundaries, such that the macroscopic velocity and pressure requirements are satisfied. These stipulations pose some difficulties in the LBM implementation. For the general pressure and velocity boundary conditions, there are usually more unknown incoming density distributions than the number of macroscopic constraint equations, i.e., more unknowns to be determined from less constraints. To have a complete system of equations, assumptions are usually necessary and inappropriate choices could lead to unphysical boundary effects and also hamper simulation stability. Tremendous efforts have been devoted to develop accurate and efficient boundary schemes for different situations (Ladd 1994b; He et al. 1997; Guo et al. 2002b; Mei et al. 1999; Zhang and Kwok 2006b; Le and Zhang 2009). Below we summarize typical boundary conditions that could be useful for microfluidic simulations.

2.4.1 Solid–Fluid boundary conditions

(a) Bounce-Back scheme for stationary no-slip boundaries

The mid-grid bounce-back scheme (Succi 2001) is typically utilized for its simplicity to model flow over a stationary no-slip boundary. In the implementation, particles leaving a boundary fluid node $\mathbf{x}_{\mathrm{b}}$ bounce back from the boundary to the original site in the reversed lattice velocity, as shown in Fig. 2):

$$f_{\bar{i}}(\mathbf{x}_{\mathrm{b}}, t+\Delta t) = f_i^*(\mathbf{x}_{\mathrm{b}}, t), \tag{12}$$

where $\mathbf{c}_{\bar{i}} = -\mathbf{c}_i$ is the reversed lattice velocity, and f_i^* represents the distribution leaving $\mathbf{x}_{\mathrm{b}}$ after collision at time t. The lattice velocity $\mathbf{c}_i$ points outward from the fluid domain at the boundary node $\mathbf{x}_{\mathrm{b}}$. This simple mechanism has been extensively utilized to model, for example, straight channel walls along the lattice grid lines. A rigorous analysis had been carried out by He et al. (1997), showing that large artificial boundary slip can be introduced by such a simple bounce-back mechanism, especially when the relaxation parameter τ is large.

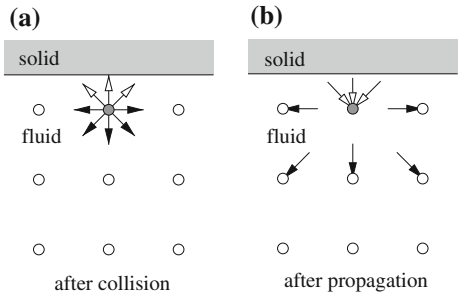

Fig. 2 Illustration of the bounce-back process on a stationary boundary. The *gray circle* is a boundary node, $\mathbf{x}_b$, and the *solid line* at the bottom of the *gray* area represents a boundary. During the propagation, three particle distributions from the boundary node $\mathbf{x}_b$, $f_2^*(\mathbf{x}_b, t)$, $f_5^*(\mathbf{x}_b, t)$, and $f_6^*(\mathbf{x}_b, t)$, are bounced back to this same node $\mathbf{x}_b$ but in reversed direction, respectively, as $f_4(\mathbf{x}_b, t + \Delta t)$, $f_7(\mathbf{x}_b, t + \Delta t)$, and $f_8(\mathbf{x}_b, t + \Delta t)$ (*open arrows*). Other distributions (*filled arrows*) follow the general propagation process and move to corresponding neighboring nodes

(b) Modified bounce-back method for moving boundaries

Simply bouncing back all outgoing particle distribution functions back to their individual origins in a reversed direction does not provide any accommodation to incorporate the boundary movement. Ladd (1994b) proposed a modification of the bounce-back scheme for moving boundaries by adding a new term to incorporate momentum injection to fluid from the moving boundary,

$$f_{\bar{i}}(\mathbf{x}_b, t + \Delta t) = f_i^*(\mathbf{x}_b, t) - \frac{2\rho w_i}{c_s^2}\mathbf{u}_b \cdot \mathbf{c}_i, \tag{13}$$

where $\mathbf{u}_b$ is the boundary velocity at the bounce-back point. With $\mathbf{u}_b = \mathbf{0}$, the last term in Eq. 13 disappears, and the original bounce-back boundary condition is recovered.

Both the original and the Ladd modified bounce-back boundary schemes assume that the boundary is located at the midpoint of the lattice link intersecting the boundary, and some loss of accuracy occurs for arbitrary boundary shapes. Aidun et al. (1998) also pointed out that the additional term in Eq. 13 violates mass conservation for the fluid and proposed a correction. These concerns are not important in most applications, and detailed discussions can be found in the literature if interested.

(c) Interpolation/extrapolation methods

The Ladd modified bounce-back boundary condition has difficulty to represent an arbitrarily curved boundary, since the boundary nodes have to be placed at the midpoints of lattice links. To overcome this shortcoming, Filippova and Hanel (1998) proposed an interpolation/extrapolation method for the unknown solid-to-fluid density distributions across curved boundaries. Here, we describe the boundary treatment with the help of Fig. 3 for a D2Q9 lattice grid. After the collision step, a fictitious distribution $f_{\bar{i}}^*$ is assumed to leave the solid node $\mathbf{x}_s$ along the lattice direction $\mathbf{c}_{\bar{i}}$ and it will arrive at the fluid node $\mathbf{x}_f$. This fictitious distribution is approximated by

$$f_{\bar{i}}^*(\mathbf{x}_s) = (1 - \chi)f_i^*(\mathbf{x}_f) + \chi f_i^*(\mathbf{x}_b) + \frac{2\omega_i\rho}{c_s^2}\mathbf{u}_b \cdot \mathbf{c}_{\bar{i}}, \tag{14}$$

where the last term is identical to that in the Ladd boundary method Eq. 13. The other two terms on the right-hand side can be interpreted as an interpolation (or extrapolation) between $f_i^*(\mathbf{x}_f)$ and $f_i^*(\mathbf{x}_b)$ with χ as a weight factor. Here, $f_i^*(\mathbf{x}_b)$ is another fictitious distribution at the boundary node $\mathbf{x}_b$ and Filippova and Hanel proposed to expressed it as (Filippova and Hanel 1998)

$$f_i^*(\mathbf{x}_b) = w_i\rho_f\left[1 + \frac{\mathbf{u}_{bf} \cdot \mathbf{c}_i}{c_s^2} + \frac{(\mathbf{u}_f \cdot \mathbf{c}_i)^2}{2c_s^4} - \frac{u_f^2}{2c_s^2}\right], \tag{15}$$

where $\rho_f = \rho(\mathbf{x}_f)$ and $\mathbf{u}_f = \mathbf{u}(\mathbf{x}_f)$. The velocity $\mathbf{u}_{bf}$ and weight factor χ are calculated from

$$\mathbf{u}_{bf} = (\Delta - 1)\mathbf{u}_f/\Delta + \mathbf{u}_b/\Delta, \quad \chi = (2\Delta - 1)/\tau \tag{16}$$

for $\Delta > 1/2$ and

$$\mathbf{u}_{bf} = \mathbf{u}_f, \quad \chi = (2\Delta - 1)/(\tau - 1) \tag{17}$$

for $\Delta \geq 1/2$.Here $\mathbf{u}_b = \mathbf{u}(\mathbf{x}_b)$ and $\Delta = |\mathbf{x}_f - \mathbf{x}_b|/|\mathbf{x}_f - \mathbf{x}_s|$ is the friction of the intersected lattice link in the fluid region (Fig. 3). Later, this method was improved by Mei et al. (1999) for a better numerical stability with $\mathbf{u}_{bf}$ and χ calculated differently when $\Delta < 1/2$:

$$\mathbf{u}_{bf} = \mathbf{u}(\mathbf{x}_{ff}), \quad \chi = (2\Delta - 1)/(\tau - 2), \tag{18}$$

where $\mathbf{x}_{ff}$ is the next inward fluid node along the lattice link, i.e., $\mathbf{x}_{ff} = 2\mathbf{x}_f - \mathbf{x}_s$ (Fig. 3).

On the other side, Guo et al. (2002b) had proposed another approach for complex solid boundaries. In this method, the required density distribution entering the fluid domain from a solid node is assumed to consist of two parts: the equilibrium and the nonequilibrium parts. The

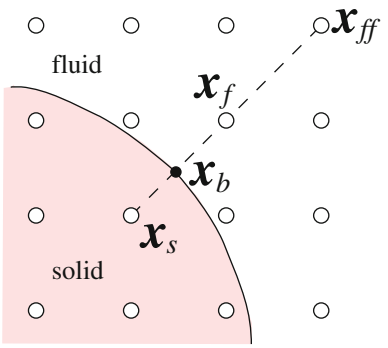

Fig. 3 Illustration of the interpolation/extrapolation boundary treatments for general boundary geometry. A lattice link between a fluid $\mathbf{x}_f$ and a solid $\mathbf{x}_s$ nodes (*dashed line*) intersects with the boundary (*curved line*) at the boundary node $\mathbf{x}_b$. $\mathbf{x}_{ff}$ is the next inward fluid node along the lattice direction

equilibrium part can be calculated using Eq. 4, where the velocity at the solid node is obtained by extrapolating from the fluid side with the required boundary velocity is enforced. Similarly, the nonequilibrium part is estimated using a first-order extrapolation with the nonequilibrium parts of distributions on the neighboring fluid nodes. Consider the illustration shown in Fig. 3. The distribution function $f_{\bar{i}}^{*}(\mathbf{x}_s, t)$ ($\bar{i} = 5$ in Fig. 3) can be expressed as (Guo et al. 2002b)

$$f_{\bar{i}}^{*}(\mathbf{x}_s, t) = f_{\bar{i}}^{\mathrm{eq}}(\mathbf{x}_s, t) + \left(1 - \frac{1}{\tau}\right) f_{\bar{i}}^{\mathrm{neq}}(\mathbf{x}_s, t), \tag{19}$$

where the equilibrium distribution

$$f_{\bar{i}}^{\mathrm{eq}}(\mathbf{x}_s, t) = f_{\bar{i}}^{\mathrm{eq}}[\rho(\mathbf{x}_s), \mathbf{u}(\mathbf{x}_s)] \tag{20}$$

using Eq. 4. The nonequilibrium distribution $f_{\bar{i}}^{\mathrm{neq}}$ is estimated by

$$f_{\bar{i}}^{\mathrm{neq}}(\mathbf{x}_s) = f_{\bar{i}}^{\mathrm{neq}}(\mathbf{x}_f), \quad \Delta \geq 0.75; \tag{21}$$

$$f_{\bar{i}}^{\mathrm{neq}}(\mathbf{x}_s) = \Delta f_{\bar{i}}^{\mathrm{neq}}(\mathbf{x}_f) + (1 - \Delta) f_{\bar{i}}^{\mathrm{neq}}(\mathbf{x}_{ff}), \quad \Delta < 0.75, \tag{22}$$

where $f_{\bar{i}}^{\mathrm{neq}}$ is the nonequilibrium part of the density distribution

$$f_{\bar{i}}^{\mathrm{neq}}(\mathbf{x}) = f_{\bar{i}}(\mathbf{x}) - f_{\bar{i}}^{\mathrm{eq}}(\mathbf{x}). \tag{23}$$

The fictitious density $\rho(\mathbf{x}_s)$ at the solid node $\mathbf{x}_s$ is usually assumed to be identical to that at the fluid node $\mathbf{x}_f$, since the density variation is small in LBM simulations for incompressible flows. The fictitious velocity $\mathbf{u}(\mathbf{x}_s)$ is calculated from those at the fluid nodes $\mathbf{x}_f$ and $\mathbf{x}_{ff}$ and the imposed boundary velocity $\mathbf{u}_b$ at the boundary point $\mathbf{x}_b$ (see Fig. 3):

$$\mathbf{u}_s = \mathbf{u}_b/\Delta + (\Delta - 1)\mathbf{u}_f/\Delta \tag{24}$$

for $\Delta \geq 3/4$ and

$$\mathbf{u}_s = \frac{3 - \Delta}{1 + \Delta}\mathbf{u}_b + (\Delta - 1)\mathbf{u}_f - \frac{(1 - \Delta)^2}{1 + \Delta}\mathbf{u}_{ff} \tag{25}$$

for $\Delta < 3/4$. Numerical simulations demonstrated a second-order numerical accuracy and better numerical stability when compared with other boundary treatments for curved boundaries (Guo et al. 2002b). It can be seen from the above descriptions that these interpolation/extrapolation methods, in principle, do not guarantee mass conservation of fluid. However, this is not important unless a large pressure gradient or body force is applied normal to the boundary (Bao et al. 2008).

(d) The immersed boundary method (IBM)

The original IBM (Peskin 1977) was developed for deformable membranes in flow field, and the membrane force can be evaluated from the membrane deformation via a constitutive relation. The membrane–fluid interaction is then accomplished by distributing membrane forces to the local fluid and by updating the membrane configuration according to local flow velocity. The attractiveness of such a treatment is that the fluid flow can be solved by appropriate numerical schemes over a fixed, regular Eulerian mesh, and therefore one can avoid the moving boundary problem. Recently, this method has been applied to study red blood cell dynamics in microcirculation (Zhang et al. 2008; Sui et al. 2008; Dupin et al. 2007). For solid boundaries, the constitutive relation is not available, and other relations have to be sought between the boundary force and desired boundary velocity. Several approaches have been proposed to simulate solid particles and moving boundaries in flows. For example, Feng and Michaelides (2004) assumed solid particles as slightly deformable with a high stiffness and the boundary force was obtained as the spring force between a particle node and its imaginary reference one. Niu et al. (2006) calculated the boundary force by the momentum exchange of the particle density distributions at boundary. In addition, Dupuis et al. (2008) recently applied an immersed boundary technique in other CFD method to LBM, which calculates the boundary force by comparing the desired boundary velocity to that computed without applying the boundary force. The immersed boundary LBM methods have been utilized in several interesting applications, such as particle suspensions (Feng and Michaelides 2004) and flow over cylinders (Dupuis et al. 2008). However, in a recent study, Le and Zhang (2009) reported the possible large deviation of boundary velocity from the imposed boundary condition, especially at high relaxation parameter values.

These solid–fluid boundary conditions have been extensively utilized, mainly in simulations of single-phase fluid systems. Recently, Joshi and Sun (2009) have integrated the Shan–Chen interparticle potential model with the Ladd mid-link boundary condition to study solid particles suspended in multiphase fluid systems. However, the Ladd boundary treatment has a low accuracy in representing a curved surface (Mei et al. 1999). On the other hand, the lack of mass conservation (Aidun et al. 1998) could become significant for particle suspensions in multiphase flows, because of the large solid–fluid interface area and the active particle motions. For these reasons, it could be interesting to examine other combinations of existing multiphase/multi-component models and boundary treatments.

2.4.2 *Open-flow boundary conditions*

Unlike the solid–fluid boundaries, open-flow boundaries are not physical interfaces, but imposed only to separate the interesting computational domain from the rest. Typical open-flow boundary conditions include inlets, outlets, periodic boundaries, and symmetry boundaries (Tu et al. 2007). In this section, we briefly outline the typical treatments for such open-flow boundaries in LBM.

(a) Inlet/outlet boundaries

The flow field inside the computational domain is typical induced by the inflow at the inlet, and controlled by the outflow at the outlet. Usually the inlet/outlet boundaries are specified as prescribed velocity and/or pressure in pairs, for example, velocity at inlet and pressure (density) at outlet, or velocity and pressure at inlet and fully developed flow at outlet (Izquierdo et al. 2009). For the first type of boundary condition with inlet velocity and outlet density available, we can simply assume the unknown distributions entering the domain as the equilibrium distributions from the inlet velocity or the outlet density, with the inlet density and outlet velocity estimated as the same as that of the next fluid node (Izquierdo et al. 2009)

$$\begin{aligned} f_i^*(\mathbf{x}_{\text{in}}) &= f_i^{\text{eq}}[\rho(\mathbf{x}_{\text{in}} + \Delta x), \mathbf{u}_{\text{in}}], \\ f_i^*(\mathbf{x}_{\text{out}}) &= f_i^{\text{eq}}[\rho_{\text{out}}, \mathbf{u}(\mathbf{x}_{\text{out}} - \Delta x)], \end{aligned} \tag{26}$$

or via a linear extrapolation from the fluid domain outward

$$\begin{aligned} f_i^*(x_{in}) &= f_i^{\text{eq}}[2\rho(x_{\text{in}} + \Delta x) - \rho(x_{\text{in}} + 2\Delta x), \mathbf{u}_{\text{in}}], \\ f_i^*(x_{\text{out}}) &= f_i^{\text{eq}}[\rho_{\text{out}}, 2\mathbf{u}(x_{\text{out}} - \Delta x) - \mathbf{u}(x_{\text{out}} - 2\Delta x)]. \end{aligned} \tag{27}$$

Here, our description is for a example situation with vertical inlet plan x_{in} at left and vertical outlet plan x_{out} at right. Alternatively, Zou and He (1997) have proposed a bounce-back scheme for the nonequilibrium distribution part, and the equilibrium part calculated from the specified boundary properties. Details of implementation of this method dependent on the particular simulation condition and can be found in the original reference (Zou and He 1997).

When the inlet boundary velocity and pressure (density) are both specified, the flow can be assumed fully developed at the outlet. For this type of inlet/outlet boundaries, Yu et al. (2005) combined the equilibrium part evaluated from the specified inlet velocity and density and the bounced back nonequilibrium part as:

$$\begin{aligned} f_i^*(x_{\text{in}}) &= f_i^{\text{eq}}(\rho_{\text{in}}, \mathbf{u}_{\text{in}}) + f_{\bar{i}}^{\text{neq}}(x_{\text{in}} + \Delta x) \\ &= f_i^{\text{eq}}(\rho_{\text{in}}, \mathbf{u}_{\text{in}}) + [f_{\bar{i}}(x_{\text{in}} + \Delta x) - f_{\bar{i}}^{\text{eq}}(x_{\text{in}} + \Delta x)], \end{aligned} \tag{28}$$

with $\bar{i}$ indicating the reverse lattice direction of i. For the outlet, Yu et al. (2005) simply used the distributions at next fluid layer

$$f_i(x_{\text{out}}) = f_i(x_{\text{out}} - \Delta x), \tag{29}$$

or it can be readily improved with a linear extrapolation:

$$f_i(x_{\text{out}}) = 2f_i(x_{\text{out}} - \Delta x) - f_i(x_{\text{out}} - 2\Delta x). \tag{30}$$

Various other treatments of inlet/outlet boundary conditions can also be found in the literature. In principle, the inlet/outlet locations should be put as far as possible from the interesting flow region. The artificial effects should also be carefully considered when interpreting the results. Sensitivity analysis, as typical in CFD practices, is recommended to ensure a reasonable accuracy (Tu et al. 2007).

(b) Periodic and symmetry boundary conditions

When a system exhibits symmetric or periodic features in space, symmetric, or periodic boundary conditions can be utilized to reduce the domain size for a better computational efficiency. Due to the particulate nature, these boundary conditions can be easily implemented in LBM. Figure 4 illustrates a horizontal symmetry boundary along the top of the domain. The basic idea is that an unknown incoming distribution across a symmetry boundary is exactly the reflection image of this required distribution about the symmetry boundary.

For periodic boundaries, all particles leaving the domain across a periodic boundary re-enter the domain from the opposite side (Fig. 4). Therefore, the actual system being simulated is then an infinitely long horizontal domain with identical repeated units. To impose a pressure gradient along the periodic direction, for example, along a channel, the periodic boundary condition can be modified to incorporate the pressure (density) drop between the domain inlet and outlet (Zhang and Kwok 2006b).

3 Multiphase/multicomponent LBM models

The dynamics of multiphase/multicomponent flows plays an important role in many areas of science and engineering, including flows through porous materials, boiling fluids, liquid metal, as well as microfludic devices. Actually, an interesting branch of microfluidics, digital, or droplet microfluidics, has been established, which focuses on the dynamic behaviors of liquid droplets in microfluidic devices (Teh et al. 2008; Fair 2007). However, simulating such complex flows numerically is challenging because of the difficulties in modeling and tracking the dynamic fluid interfaces. Also it should be noted that the solid–fluid interfacial effects (for example, surface wettability), which are consequences of microscopic solid–fluid interactions, become profound to the droplet dynamics.

As a mesoscopic simulation method describing macroscopic flows by dealing with the underlying microphysics (Sehgal et al. 1999), it is relatively easier to incorporate intermolecular interactions, which is the physical origin of phase separation, interfacial tensions, and surface wettability in multiphase/multicomponent fluid systems. For these reasons, LBM possesses several advantages over other numerical methods, and it has been demonstrated to be a useful alternative for such complex situations by numerous practices (e.g., Kang et al. 2002; Briant et al. 2004; Zhang and Kwok 2006a; Hyvaluoma et al. 2007;

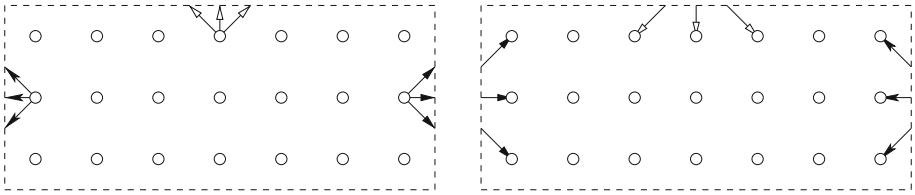

Fig. 4 Illustration of the symmetric (*top boundary*) and periodic(*left* and *right boundaries*) boundary conditions. During the propagation step, particle distributions leaving the domain across the left (or right) boundary will re-enter the domain from the right (or left) side (*filled arrows*), because of periodicity in the horizontal direction. For the symmetric boundary on top, the distributions are simply reflected as shown by the *open arrows*

Wolf et al. 2009; Liu and Zhang 2009; Verberg et al. 2004; Horbach and Succi 2006; Sbragaglia et al. 2006; Harting et al. 2006). Different from some traditional CFD interface treatments, such as those in VOF and the level set methods, the LBM multiphase/multicomponent algorithm is uniform throughout the entire domain and phase separation as well as interface evolution can be obtained without front-capturing and front-tracking treatments. Many LBM models have been proposed (Gunstensen et al. 1991; Shan and Chen 1993, 1994; Swift et al. 1995, 1996; Luo 1998; He et al. 1999; Inamuro et al. 2003; Zhang et al. 2004; Zhang and Kwok 2009). Among them, two representative approaches, the interparticle potential and the free energy models, will be introduced in this section for their extensive applications in microfluidics. Several other models will also be briefly reviewed.

3.1 The interparticle potential models

To incorporate the microscopic interactions among fluid particles and therefore generate phase separation, Shan and Chen (1993, 1994) proposed to adopt a pairwise interparticle potential among the conceptual fluid particles in LBM. Similar to the general treatment in MD, this model assumes that the fluid particles are experiencing interactions from its neighbors. For single component nonideal fluids, an attractive force is introduced as (Shan and Chen 1994):

$$\mathbf{F}(\mathbf{x}) = -\psi(\mathbf{x}) \sum_i g_i G \psi(\mathbf{x} + \mathbf{c}_i)\mathbf{c}_i, \tag{31}$$

where $\psi(\mathbf{x}) = \psi[\ \rho(\mathbf{x})]$ plays a role as the effective density, G is the attraction strength, and g_i are weight factors dependent on the lattice structures employed (Benzi et al. 2006a; Raiskinmaki et al. 2000). For the D2Q9 lattice model, we have $g_0 = 0$, $g_{1-4} = 1$, and $g_{5-8} = 1/4$. These specific factors come from projecting the interaction potential from a 4D FCHC (face-center hyper-cubic) lattice to the D2Q9 lattice model such that to ensure the interface isotropy (Yang et al. 2000; Kang et al. 2002). Actually, the above equation can be considered as a discrete version of the force evaluation from interaction potential over the lattice grid (Shan and Chen 1993; Zhang and Tian 2008). To reflect the momentum change caused by such a force at each time step, an equilibrium velocity $\mathbf{u}^{\mathrm{eq}}$ was defined as in Eq. 10 and it is utilized to calculate the equilibrium distribution f_i^{eq} through Eq. 4. After such a treatment, the relationship of pressure and density in the resulting Navier–Stokes equation has a pressure term expressed as

$$P = c_s^2 \rho + \frac{3c_s^2 G}{2}\psi^2. \tag{32}$$

This can be considered as the equation of state (EOS) of a nonideal fluid, which makes a liquid-vapor phase separation possible, as demonstrated in numerous simulations (Shan and Chen 1993; Yang et al. 2000; Hou et al. 1997). Analysis has shown that $\psi(\rho) = \psi_0 e^{-\rho_0/\rho}$ (ψ_0 and ρ_0 are constants during a simulation) is the only functional form that is consistent with continuum thermodynamics (Shan and Chen 1994; Succi 2001). However, a simpler relation $\psi = \rho$ is also commonly utilized in practical applications (Fan et al. 2001). Recently, the issue of the thermodynamic consistency of the Shan–Chen model has been further examined, and a connection between the Shan–Chen interparticle potential model and the free energy approach has been established (Shan 2008; Sbragaglia et al. 2009; Benzi et al. 2009).

One important feature of this LBM multiphase model is that phase separation is achieved automatically from the interactions, if only the interaction strength G exceeds a critical value. This means that the strength G has an inverse effect as temperature in the van der Waals theory of phase separation (Shan and Chen 1994). On the other hand, the interaction strength G also determines the resulting interfacial tension, and hence leaves less flexibility for users to adjust the density ratio and interfacial tension simultaneously (Sbragaglia et al. 2007). To address this point, Sbragaglia et al. (2007) had extended the interparticle interaction potential to a wider range, for example, to the next-nearest neighboring lattice nodes:

$$\mathbf{F}(\mathbf{x}) = -\psi(\mathbf{x}) \sum_i g_i [G_1 \psi(\mathbf{x} + \mathbf{c}_i) + G_2 \psi(\mathbf{x} + 2\mathbf{c}_i)] \mathbf{c}_i, \tag{33}$$

and the resulted EOS would be

$$P = c_s^2 \rho + \frac{3c_s^2 (G_1 + 2G_2)}{2} \psi^2. \tag{34}$$

Here, the interaction strength factors G_1 and G_2 can be utilized to tune the EOS and surface tension independently of each other. For example, by holding $G_1 + 2G_2$ constant but varying the individual values of G_1 and G_2, the liquid-vapor interfacial tension can be adjusted with the same bulk coexistence densities (Sbragaglia et al. 2007).

It has been noticed that the EOS Eq. 8 from the Shan–Chen model is a combination of the ideal gas law and the interaction contribution to pressure, similar to that in the well-known van der Waals equation. However, the exclusion-volume effect of nonideal fluid was absent in the interparticle potential model (Zhang and Tian 2008). As a result, the particular form of Eq. 32 prohibits its direct application to model realistic nonideal fluids with various EOSs. To overcome such a difficulty, Qin (2006, 2007) and Yuan and Schaefer (2006) proposed to modify the interparticle potential to obtain a desired EOS. Such an approach lumped the contributions from the particle exclusion-volume effect and the interparticle interactions together, and thus the unique physical representation of the interparticle potential in the Shan–Chen model was aborted. Moreover, computational difficulty may also arise in some particular situations in the interfacial region (Zhang and Tian 2008). To incorporate the missing exclusion-volume effect, recently Zhang and Tian (2008) utilized a generalized version of the equilibrium distribution, which consists a parameter representing the portion of rest particle when the fluid is stationary. When comparing this revised Shan–Chen model to the general LBM algorithm, the two different points, i.e., the interparticle interaction and the rest particle portion, clearly represent the two major effects that differentiate a nonideal fluid from an ideal one. In addition, the interparticle potential can be physically interpreted as a discrete representation of the intermolecular attraction with the *effective density* $\psi(\rho)$ replaced with the *physical* density ρ itself (Zhang and Tian 2008).

Similar treatment has also been applied to simulate immiscible multicomponent fluids (Shan and Chen 1993; Shan and Doolen 1995). Multiple sets of density distribution functions are employed for individual components and these distribution functions evolve according to their individual LBEs. Again fluid–fluid interactions are introduced to generate phase separation between different fluid components. Typically, the fluid–fluid interactions are only considered for unlike fluid particles and the force is set as repulsive to ensure a phase separation (Kang et al. 2002; Shan and Chen 1993; Shan and Doolen 1995). As a result, fluids in such simulations behave as ideal gases in the bulk phase, where the fluid density of individual component is nearly constant and therefore interaction forces are cancelled out. For simplicity, most simulations usually only include the interactions between nearest neighbors.

3.2 The free energy models

To avoid the thermodynamic inconsistency and to improve the spurious velocity in the interfacial region, Swift et al. (1995, 1996) implemented an equilibrium pressure tensor for a nonideal fluid into the collision operator by reconstructing the equilibrium distribution f_i^{eq}. The free energy model started from the van der Waals formulation of quasi-local thermodynamics for a two-component fluid in thermodynamic equilibrium at a temperature T with the fluid free energy F expressed as (Swift et al. 1995)

$$F(\mathbf{x}) = \int \left\{ \psi[\rho(\mathbf{x})] + \frac{\kappa}{2} |\nabla \rho(\mathbf{x})|^2 \right\} \mathrm{d}\mathbf{x}. \tag{35}$$

The first term in the integral $\psi(\rho)$ describes the bulk free energy density, which depends on the fluid EOS. The second term accounts for the contribution from any density gradients. Here, κ is a parameter representing the fluid–fluid interactions. Such an expression of the fluid free energy is called the squared-gradient approximation. The full pressure tensor has the following form

$$\mathbf{P} = \left[\rho \psi'(\rho) - \psi(\rho) - \kappa \rho \nabla^2 \rho - \frac{\kappa}{2} (\nabla \rho)^2 \right] \mathbf{I} + \kappa \nabla \rho (\nabla \rho)^T. \tag{36}$$

The first two terms in the square brackets above are actually the EOS of the fluid. In order to incorporate the above formulation into the general LBM algorithm, the equilibrium distribution f_i^{eq} was reconstructed as (Briant et al. 2004)

$$f_i^{\mathrm{eq}} = A_i + B_i \mathbf{u} \cdot \mathbf{c}_i + C_i u^2 + D_i (\mathbf{u} \cdot \mathbf{c}_i)^2 + \mathbf{G}_i : \mathbf{c}_i \mathbf{c}_i^T, \tag{37}$$

where the coefficients A_i, B_i, C_i, D_i, and the elements of matrix $\mathbf{G}_i$ can be determined from the conservation of mass, momentum and the momentum flux tensor constraint:

$$\begin{aligned} &\sum f_i^{\mathrm{eq}} = \rho, \\ &\sum f_i^{\mathrm{eq}} \mathbf{c}_i = \rho \mathbf{u}, \\ &\sum_i f_i^{\mathrm{eq}} \mathbf{c}_i \mathbf{c}_i^T = \mathbf{P} + \rho \mathbf{u} \mathbf{u}^T. \end{aligned} \tag{38}$$

The detailed expressions of these coefficients can be found in the literature for the D2Q9 (Briant et al. 2004) and D3Q15 (Dupuis and Yeomans 2004) lattice models.

A similar multicomponent model based on the above free energy approach is also available (Swift et al. 1996; Wagner and Yeomans 1999; Briant and Yeomans 2004). For a binary system, two sets of distribution functions are utilized: one for the fluid flow and the other for the density difference between the two components. The corresponding two relaxation parameters are related to the fluid viscosity and the mobility coefficient of the density difference. In order to generate a phase separation between the two components, a free energy function of the density difference was designed with two local minimums (Swift et al. 1996; Wagner and Yeomans 1999; Briant and Yeomans 2004). However, as pointed out by Li and Wagner (2007), this free energy approach for fluid density-differences is in general asymmetric. For example, when simulating a ternary fluid system, three sets of density distributions for, respectively, the total density, the density of a particular component, and the density deviation from the average density of another component. Clearly this choice is sort of arbitrary and is likely to be asymmetric because the three components are treated differently (Li and Wagner 2007). To address this issue, similar to the interparticle potential model for multicomponent systems (Shan and Chen 1993; Shan and Doolen 1995), Li and Wagner (2007) thus proposed to model each component with its individual density distributions instead of differences among them.

Sullivan (1981) had criticized the squared-gradient version of the van der Waals theory (Cahn and Hilliard 1958; Fisk and Widom 1969) as phenomenological, since it failed to relate directly the properties of nonuniform fluid to the interactions occurring at a molecular level. It had also been shown that the gradient expansion approximation, which is used in deriving the squared-gradient theory, would no longer be valid when an impenetrable solid boundary presents (Sullivan 1981; Widom 1978). In applications of the squared-gradient free energy LBM model to situations with solid surfaces, different treatments, either by an external chemical potential (Swift et al. 1995) or the Cohn surface free energy (Briant et al. 2004; Kusumaatmaja et al. 2006; Dupuis et al. 2008), can be found. The latter approach, which is often employed in recent years, had also been criticized by Sullivan (1981). For a better representation of the microscopic interactions, Zhang et al. (2004) proposed another free energy approach with a mean-field expression of the nonlocal free energy term. This model incorporates the solid–fluid interaction effects naturally and physically, as demonstrated by the fluid density distribution near and contact angle on a solid surface (Zhang et al. 2004). Li and Tafti (2007) have pointed out that the original mean field pressure expression might not be complete. However, their pressure deviation started from a thermodynamic relation for homogeneous fluids, which is not suitable for inhomogeneous fluids, for example, with interfaces (Rowlinson and Widom 1982; Yang et al. 1976). Recently, this mean field free energy approach has also been extended to multicomponent systems recently (Zhang and Kwok 2009). Simulations for a ternary fluid system showed that both the global free energy and the microscopic interactions among fluid components had been well represented.

3.3 Other multiphase/multicomponent models

A notable problem with these physics-originated models is that the density difference between different phases is usually limited when compared to realistic systems. For example, the water density is $\sim$1000 times of that of air. To address this point, people apply treatments similar to those in other traditional CFD methods and several high-density-ratio models have been proposed (Inamuro et al. 2004a; Lee and Lin 2005b; Zheng et al. 2006). For example, Inamuro et al. (2004a) adopted a free energy approach for the flow velocity and order parameter, and solved the pressure field from a Poisson equation as in general CFD methods. Another point is that the interface thickness from these models is usually orders larger than the actual thickness. This is not surprising, since several lattice units are needed to represent the property (e.g., density) change from one phase to another. Some models have also been proposed by treating the interface as an artificial boundary (Ginzburg and Steiner 2003; Korner et al. 2005). These models require extra sets of distribution functions or more complicated interface treatments, and the computational efficiency has to be somewhat sacrificed. Also the phase-separation from these models has less physical basis and is more phenomenological. For applications in microfluidics where the physical microscopic interactions are important (e.g., dynamic wetting), carefulness should be executed when interpreting the simulation results. Moreover, these approaches, although attractive from a practical point of view, blur the distinction between LBM and other traditional CFD methods for multiphase fluid systems.

4 LBM-like algorithms for other processes and phenomena

Realizing that the LBM dynamics can be viewed as a numerical solver of differential equations, several LBM-like algorithms have been proposed to solve problems that can be described by similar differential equations. Such algorithms are designed so that the corresponding macroscopic differential equations can be recovered through a Chapman–Enskog analysis. However, we should be aware that these models are purely numerical solvers, and the *density distributions* in these models have no physical

meaning as those in the original LBM for fluid mechanics. In this section, we introduce several such models for heat transfer, electrical field, magnetic field, and diffusion process for their potential applications in microfluidic systems.

4.1 LBM models for heat transfer

Many flow systems involve heat transfer, both at macroscopic and at microscopic scales (e.g., the Joule heating effect, Li 2004). To include the thermal effects in flow simulation, three typical approaches have been developed within the general LBM framework: the multispeed, passive scalar, and double distribution approaches (Peng et al. 2003; Wang et al. 2007a; Meng et al. 2008; Chatterjee 2009). The multispeed models can be considered as extensions of the general isothermal LBM method by ensuring local energy conservation with more discrete lattice velocities at a fluid node (Alexanders et al. 1993; Chen 1994). This approach exhibits severe numerical instabilities and therefore the simulated temperature can only vary in a narrow range (Peng et al. 2003; Wang et al. 2007a; Chatterjee 2009). By taking advantage of the formal analogy between heat and mass transfer, the passive scalar approach considers the temperature as a scalar property, and its evolution is simulated similarly by another set of distribution functions using two-component LBM models (Shan 1997; Inamuro et al. 2002). The numerical stability has been improved, however, as firstly pointed out by He et al. (1998), the viscous dissipation and compression work were not incorporated. He et al. therefore developed the double distribution scheme with one for the flow field and another for the internal energy density. In addition, D'Orazio and Succi (2004) have developed thermal boundary conditions for the doubled distribution model with the Dirichlet and Neumann boundary constraints. Below, we present the double distribution thermal model briefly. In this thermal LBM model, two LBEs are employed:

$$\begin{aligned}
&\bar{f}_i(\mathbf{x}+\mathbf{c}_i\Delta t, t+\Delta t)-\bar{f}_i(\mathbf{x},t)\\
&=-\frac{1}{\tau_f+1/2}\left[\bar{f}_i(\mathbf{x},t)-\bar{f}_i^{\mathrm{eq}}(\mathbf{x},t)\right],\\
&\bar{g}_i(\mathbf{x}+\mathbf{c}_i\Delta t, t+\Delta t)-\bar{g}_i(\mathbf{x},t)=\\
&-\frac{1}{\tau_g+1/2}[\bar{g}_i(\mathbf{x},t)-\bar{g}_i^{\mathrm{eq}}(\mathbf{x},t)]-\frac{\tau_g}{\tau_g+1/2}f_iZ_i\Delta t,
\end{aligned} \tag{39}$$

where the distributions $\bar{f}_i$ and $\bar{g}_i$ are related to the fluid f_i and internal energy distributions g_i as

$$\begin{aligned}
\bar{f}_i &= f_i+(f_i-f_i^{\mathrm{eq}})/2\tau_f,\\
\bar{g}_i &= g_i+(g_i-g_i^{\mathrm{eq}})/2\tau_g+f_iZ_i\Delta t/2.
\end{aligned} \tag{40}$$

Also two relaxation parameters, τ_f and τ_g, have been introduced for $\bar{f}_i$ and $\bar{g}_i$, respectively. The fluid equilibrium distribution f_i^{eq} is calculated from Eq. 4 as before, while the internal energy equilibrium distribution g_i^{eq} is expressed as

$$\begin{aligned}
g_0^{\mathrm{eq}} &= w_0\rho e\left(-\frac{u^2}{2c_s^2}\right),\\
g_i^{\mathrm{eq}} &= w_i\rho e\left[\frac{3}{2}+\frac{\mathbf{c}_i\cdot\mathbf{u}}{2c_s^2}+\frac{(\mathbf{c}_i\cdot\mathbf{u})^2}{2c_s^4}-\frac{u^2}{2c_s^2}\right]\quad(i=1\text{–}4),\\
g_i^{\mathrm{eq}} &= w_i\rho e\left[3+\frac{2\mathbf{c}_i\cdot\mathbf{u}}{c_s^2}+\frac{(\mathbf{c}_i\cdot\mathbf{u})^2}{2c_s^4}-\frac{u^2}{2c_s^2}\right]\quad(i=5\text{–}8).
\end{aligned} \tag{41}$$

The viscous dissipation effect is incorporated by Z_i in Eqs. 39 and 40, given by

$$Z_i=(\mathbf{c}_i-\mathbf{u})\cdot\left[\frac{\partial\mathbf{u}}{\partial t}+(\mathbf{c}_i\cdot\nabla)\mathbf{u}\right]. \tag{42}$$

The fluid kinematic viscosity v and thermal diffusivity D are used to determine the relaxation parameters τ_f and τ_g, respectively, via

$$v=\tau_fc_s^2\Delta t,\quad D=2\tau_gc_s^2\Delta t. \tag{43}$$

The corresponding energy equation can be obtained via a Chapman–Enskog analysis based on the above algorithm with the macroscopic internal energy e and heat flux $\mathbf{q}$ expressed as (He et al. 1998)

$$\begin{aligned}
e &= \sum_i(\bar{g}_i-f_iZ_i\Delta t/2)/\rho,\\
\mathbf{q} &= \frac{\tau_g}{\tau_g+1/2}\left(\sum_i\mathbf{c}_i\bar{g}_i-\rho e\mathbf{u}-\sum_i\mathbf{c}_if_iz_i\Delta t/2\right).
\end{aligned} \tag{44}$$

4.2 LBM models for electric field

Eletrokinetic phenomena are extensively utilized in microfluidic systems to induce, control, and manipulate liquid motions (Li 2004; Zagnoni et al. 2009). In such situations, the fluid flow and electrical field are highly coupled and therefore they should be solved simultaneously in simulations. Several LBM-like algorithms have been developed to solve the governing Poisson–Boltzmann equation (Warren 1997; He and Li 2000; Guo et al. 2005; Wang et al. 2006). Guo et al. (2005) had provided a complete overview of existing LBM models for electrical potential field. Here, we represent the model proposed by He and Li (2000) for its simplicity.

Generally, the electric potential ϕ over space is governed by the Poisson equation

$$\nabla\cdot(\epsilon\nabla\phi)=-\frac{\rho_e}{\epsilon_0}, \tag{45}$$

where ε and ε_0 are, respectively, the dielectric constant of the medium and the permittivity of the vacuum, and ρ_e is

the net charge density, which can be related to the electric field through the Boltzmann distribution in an electrolyte (Li 2004). To solve this equation in the framework of LBM, He and Li (2000) proposed the following LBE for density distribution h_i

$$h_i(\mathbf{x}+\mathbf{c}_i\Delta t, t+\Delta t) - h_i(\mathbf{x},t) = -\frac{h_i(\mathbf{x},t) - h_i^{\mathrm{eq}}(\mathbf{x},t)}{\tau_\phi} + \frac{w_i\rho_e}{\epsilon_0}. \quad (46)$$

The corresponding equilibrium distribution h_i^{eq} is related to the electrical potential ϕ via the lattice weight factor w_i by

$$h_i^{\mathrm{eq}} = w_i\phi \quad (47)$$

and the relaxation parameter τ_ϕ is determined from the dielectric constant ϵ_i as

$$\tau_\phi = 3\epsilon + 0.5. \quad (48)$$

The interested electrical potential ϕ is just a sum of all potential distribution h_i, i.e.,

$$\phi = \sum_i h_i. \quad (49)$$

Again the Chapman–Enskog analysis can be applied to Eq. 46 and the following macroscopic equation

$$\frac{\partial\phi}{\partial t} = \nabla\cdot(\epsilon\nabla\phi) + \frac{\rho_e}{\epsilon_0} \quad (50)$$

can be obtained (Guo et al. 2005). Therefore, the original Poisson equation can be approximated at the steady state limit (He and Li 2000; Guo et al. 2005).

4.3 LBM models for magnetic field

Magnetic fields are also often employed in microfluidic devices for flow pumping, controlling, and mixing. Within the LBM framework, several model have been developed to solve the magnetic field (Chen et al. 1991; Succi et al. 1991; Dellar 2002; Breyiannis and Valougeorgis 2004). Among them, Dellar (2002) modeled the magnetic field with a set of *vector* distribution functions, and they obey a LBGK-type evolution equation. Compared to previous multi-speed models, this method has advantages in reduced computation requirement and independent adjustment of the fluid viscosity and magnetic diffusivity (Dellar 2002; Breyiannis and Valougeorgis 2004). In MHD, the magnetic induction equation is written as

$$\frac{\partial\mathbf{B}}{\partial t} + \nabla\cdot(\mathbf{uB} - \mathbf{Bu}) = \eta\nabla^2\mathbf{B}, \quad (51)$$

where $\mathbf{B}$ is the magnetic induction field and η is the magnetic resistivity or diffusivity (Dellar 2002; Pattison et al. 2008). In addition, the solenoidal divergence-free constraint

$$\nabla\cdot\mathbf{B} = 0 \quad (52)$$

is imposed (Breyiannis and Valougeorgis 2004; Dellar 2002). The magnetic effect on flow field is represented by the Lorenz force and the general Navier–Stokes equation is modified to

$$\frac{\partial\mathbf{u}}{\partial t} + (\mathbf{u}\cdot\nabla)\mathbf{u} = -\frac{1}{\rho}\nabla p + \nu\nabla^2\mathbf{u} + \frac{1}{\rho}\mathbf{J}\times\mathbf{B}, \quad (53)$$

where $\mathbf{J} = \nabla\times\mathbf{B}$ is the current density. To solve this equation, a vector distribution function $\mathbf{g}_i$ is introduced, which obeys the following LBE

$$\bar{\mathbf{g}}_i(\mathbf{x}+\mathbf{c}_i\Delta t, t+\Delta t) - \bar{\mathbf{g}}_i(\mathbf{x},t) = -\frac{\Delta t}{\tau_m + \Delta t/2}\times[\bar{\mathbf{g}}_i(\mathbf{x},t) - \mathbf{g}_i^{\mathrm{eq}}(\mathbf{x},t)], \quad (54)$$

where the new distribution $\bar{\mathbf{g}}$ is related to $\mathbf{g}$ by

$$\bar{\mathbf{g}}_i(\mathbf{x},t) = \mathbf{g}_i(\mathbf{x},t) + \frac{\Delta t}{2\tau_m}[\mathbf{g}_i(\mathbf{x},t) - \mathbf{g}_i^{\mathrm{eq}}(\mathbf{x},t)] \quad (55)$$

and the equilibrium distribution $\mathbf{g}_i^{\mathrm{eq}}$ is expressed as (Chen and Shi 2005)

$$\mathbf{g}_i^{\mathrm{eq}} = w_i\left[\mathbf{B} + \frac{\mathbf{c}_i\cdot(\mathbf{uB} - \mathbf{Bu})}{c_s^2}\right]. \quad (56)$$

The magnetic field $\mathbf{B}$ can be obtained by summing the distributions $\mathbf{g}_i$ as

$$\mathbf{B} = \sum_i \mathbf{g}_i, \quad (57)$$

and the magnetic diffusivity η is related to the relaxation parameter τ_m as $\eta = \tau_m\Delta t/c_s^2$. Typically the D2Q4 (2D and four lattice velocities) or D2Q5 (2D and five lattice velocities) lattice structures are utilized for 2D systems (Dellar 2002), and the D3Q7 (3D and seven lattice velocities) model can be adopted for 3D flows (Breyiannis and Valougeorgis 2004). The lattice weight factors here are chosen as $w_0 = 1/3$ and $w_{1-4} = 1/6$ for the D2Q5 model, and $w_{1-4} = 1/4$ for the D2Q4 model (Dellar 2002). The original magnetic induction equation (51) can be recovered correctly from a Chapman–Enskog analysis (Dellar 2002), and the current density $\mathbf{J} = \nabla\times\mathbf{B}$ can be computed either from macroscopic quantities or, more consistently, from higher moments of the magnetic density distribution $\mathbf{g}_i$ (Dellar 2002; Breyiannis and Valougeorgis 2004), and the Lorenz force can then be incorporated in the Navier–Stokes equation.

4.4 LBM models for diffusion processes

Convection-diffusion processes are often encountered in various flow situations, including microfluidic systems (Li

2004; Weigl and Yager 1999). Such a process is governed by the well-known convection-diffusion equation

$$\frac{\partial c}{\partial t} = D\nabla^2 c - \mathbf{u}\cdot\nabla c + S(\mathbf{x},t), \tag{58}$$

where c represents the concentration of the interested substance, D is the diffusion coefficient, and S is the source term due to possible reaction. The flow velocity $\mathbf{u}$ can be obtained from, for example, the LBGK method for fluid dynamics described in Sect. 2.1. To solve the convection-diffusion equation (58) within the LBM framework, several models have been proposed (Dawson et al. 1993; Guo et al. 1999; He et al. 2000). Recently, Shi et al. (2008a) proposed a new scheme for the source term in the LBE for a better accuracy.

In this model, a distribution function j_i is introduced, which is updated according to the following LBE

$$j_i(\mathbf{x}+\mathbf{c}_i\Delta t, t+\Delta t) - j_i(\mathbf{x},t) = -\frac{j_i(\mathbf{x},t) - j_i^{\mathrm{eq}}(\mathbf{x},t)}{\tau_c} + \Delta t S_i + \frac{\Delta t^2}{2}\bar{D}_i S_i, \tag{59}$$

where τ_c is a relaxation parameter and it is related to the diffusion coefficient D by

$$D = \frac{2\tau_c - 1}{2}\Delta t c_s^2. \tag{60}$$

The effect of the source term S in Eq. 58 is incorporated in the above LBE Eq. 59 by

$$S_i = \left(1 + \frac{2\tau_c - \mathbf{c}_i\cdot\mathbf{u}}{2\tau_c - \theta c_s^2}\right) w_i S, \tag{61}$$

and $\bar{D}_i = \partial_t + \theta\mathbf{c}_i\cdot\nabla$. Here, $\theta \in [0, 1]$ is a parameter for different difference schemes (Shi et al. 2008a). The equilibrium distribution j_i^{eq} is expressed simply as

$$j_i^{\mathrm{eq}} = w_i c, \tag{62}$$

and the concentration c can be calculated from the distribution functions j_i by

$$c = \sum_i j_i. \tag{63}$$

Through a Chapman–Enskog analysis (Shi et al. 2008a), the convection-diffusion equation (58) can be recovered correctly from the above LBM algorithm.

In addition, LBM-like models for other situations, such as porous flows (Martys 2001; Guo and Zhao 2002; Freed 1998), axisymmetric flows (Huang and Lu 2009; Guo et al. 2009; Reis and Phillips 2007), uniform channel flows (Xiong and Zhang 2010b), and shallow water flows (Liu et al. 2009; Klar et al. 2008), are also available. These models might be useful for microfluidic simulations and interested readers can refer the above references and those therein.

5 Applications in microfluidics

In recent years, as in other fluid-related areas, LBM has been extensively applied to study various transport phenomena and processes in microfluidic systems. Examples include microscopic gaseous flows, electroosmotic flows, interfacial phenomena, microscopic biofluidics, and colloid suspensions. In this section, we review some representative applications of LBM in these areas.

5.1 Microscopic gaseous flows

Micro-electro-mechanical-systems (MEMS) have experienced rapid progress in recent years for their applications in various areas, including automotive, aerospace, medical devices, and telecommunications. In such microscopic systems, gaseous flows are commonly involved and their behaviors are important to the system performance (Ho and Tai 1998; Gad-el-Hak 1999). The Knudsen number $K_n = \lambda/L$, the ratio of the gas mean free path λ to a characteristic length of the flow domain L, usually serves as a criterion in determining whether the continuum assumption is applicable to a fluid flow. By definition, the mean free path is the average distance traveled by a gas molecule between two subsequent collisions with other molecules. The mean free path is usually in a range of 20–200 nm. Several flow regimes can be classified according to the Knudsen number (Gad-el-Hak 1999). For flows in large domains with $K_n \leq 10^{-3}$, the general Navier–Stokes equation and no-slip boundary are reasonable to describe the flow behaviors, as we do in most macroscopic situations. As the flow domain becomes smaller, the Knudsen increases, and some rarefaction effects, such as velocity slip and temperature jumps on solid boundaries, have been observed. For the slip flow regime of $10^{-3} \leq K_n \leq 10^{-1}$, the Navier–Stokes equation is still applicable in the bulk region; however, slip boundary condition has to be considered over the solid boundaries. For the transition ($10^{-1} \leq K_n \leq 10$) and free-molecule ($K_n > 10$) flows, the particulate and kinematic nature of the gas becomes dominant, and the Boltzmann equation is necessary to analyze such flows.

Microscopic gaseous flows in MEMS are usually in the slip and transition regimes. As LBM can be considered as a numerical solver of the Navier–Stokes equation and also a discretized version of the Boltzmann equation, it appears that LBM should be an attractive choice for these microflows (Guo and Zheng 2008; Verhaeghe et al. 2009). Indeed, several attempts have been made since 2002. These models usually take the various LBM formulations, including the simple LBGK model (Nie et al. 2002; Lim et al. 2002; Agrawal et al. 2005; Chai et al. 2008), the MRT model (Verhaeghe et al. 2009; Guo et al. 2008), the

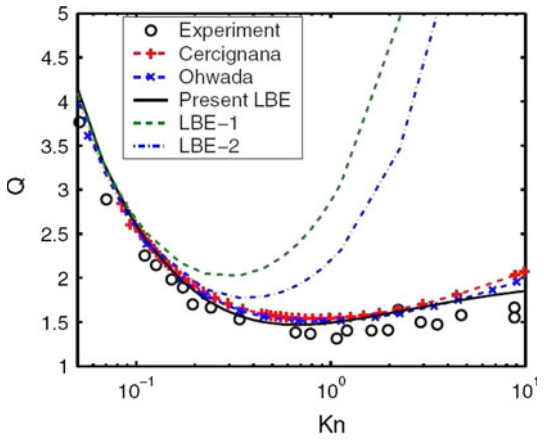

Fig. 5 Simulated mass flow rate Q of gaseous Poiseuille flows with different Knudsen numbers from the LBM model by Guo et al. (2008) (*solid line*). The Knudsen minimum has been successfully captured at $Kn \cong 0.5$. See the original reference for the legend details. Reprinted with permission from Guo et al. (2008). Copyright 2008 by the American Physical Society

high-order lattice structures (Zhang et al. 2006; Kim et al. 2008), and the entropy LBM model (Tang et al. 2007b), as a flow solver for the bulk fluid region, and adopt particular boundary treatments that allow a relative slip between fluid and surface. In general, the relaxation time τ need to be related to the Knudsen number K_n to reflect the connection between the fluid viscosity and the mean free path according to the kinetic theory (Nie et al. 2002). Various such $\tau \sim K_n$ relationships have been proposed from different viewpoints (Nie et al. 2002; Lim et al. 2002; Sbragaglia and Succi 2005; Zhang et al. 2005b). The effects of local flow situation and wall boundary on the relaxation time have also been considered (Tang et al. 2008; Guo et al. 2007, 2008). Moreover, Guo et al. (2006, 2007) have pointed out that the relaxation time should satisfy one basic consistency requirement: in the continuum limit $K_n \to 0$, the relation between the dynamic viscosity and the relaxation time $\mu = \tau p$ should be fulfilled. Meanwhile, the general no-slip boundary condition has to be replaced some more complicated schemes to achieve the boundary slip for microscopic gaseous flows. Again different boundary treatments have been reported, including the bounce-back boundary condition (Nie et al. 2002; Agrawal et al. 2005; Zhang et al. 2006), the specular reflection method (Lim et al. 2002), the diffusive scattering boundary (Ansumali and Karlin 2002; Niu et al. 2004; Sofonea and Sekerka 2005; Tang et al. 2007b), the equilibrium boundary (Lee and Lin 2005a), and various combinations of them (Verhaeghe et al. 2009; Succi 2002; Chai et al. 2008; Guo et al. 2008; Tang et al. 2005). It has been shown that the boundary slip from a pure bounce-back scheme is a numerical artifact (He et al. 1997) and cannot reflect the physical slip over the surface. Therefore, the suitable choices should be other methods or their combinations. Guo et al. (2007) have examined these different boundary treatments and pointed out that the combination of the bounce-back and specular-reflection schemes and the diffusive scattering scheme are virtually equivalent and there exist discrete effects in both the schemes.

Good agreement has been observed in these LBM simulations when compared with other studies. For example, the Knudsen minimum of the gaseous flow rate in channel, which is a key character of microscopic gaseous flows, has been successfully reproduced in several LBM simulations (Guo et al. 2008; Zhang et al. 2005a; Ansumali et al. 2006; Zhang et al. 2006) (Fig. 5). However, these simulations were usually limited to simple geometry structures like two-dimensional straight channels. Chai et al. (2008) have simulated gaseous microflows in rough microchannels with regular rectangular structures. Also Liu and Ni (2008) have investigated the roughness effect on gas flows, with the channel surfaces modeled as a pair of self-affine fractal walls. The boundary treatments adopted for these rough surfaces were similar to those for flat surfaces: a combination of the bounce-back and full diffusive schemes (Chai et al. 2008), or a combination of the bounce-back and reflection schemes (Liu and Ni 2008). It should be noted that both the bounce-back and the specular reflection schemes assume that the physical boundary, i.e., the bouncing-back or reflecting point, locates at the midpoint

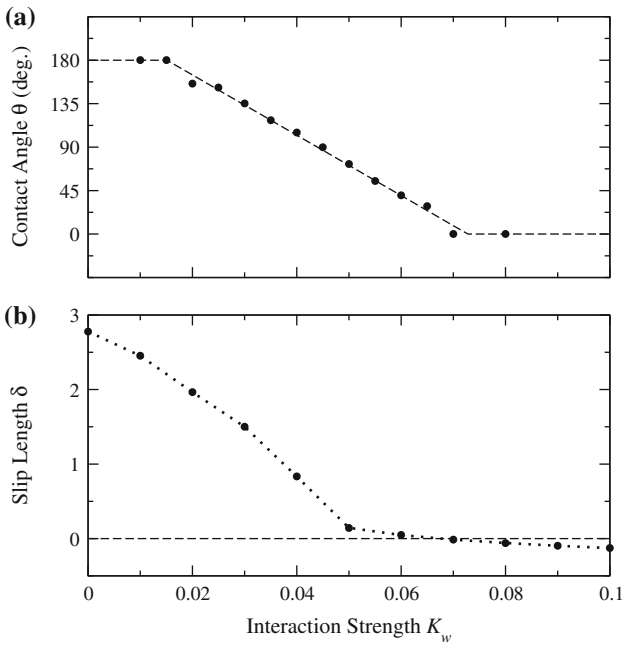

Fig. 6 Simulated contact angle (**a**) and slip length (**b**) with different solid-fluid interaction strength from the mean field free energy LBM model. The general trend of large slip over hydrophobic surfaces has been successfully reproduced. Reprinted with permission from Zhang and Kwok (2004a). Copyright 2004 by the American Physical Society

of the lattice link crossing the boundary. Therefore, when modeling surface roughness of small magnitude using such treatments, the inaccuracy introduced could be large, and this effect deserves further investigation. Possible improvement could be to develop more accurate boundary conditions, for example, using the interpolation/extrapolation technique (Filippova and Hanel 1998; Mei et al. 1999; Guo et al. 2002b), or to utilize the adaptive mesh refinement (Toolke et al. 2006). Moreover, the boundary slip velocity in most of these models was specified in the boundary treatments as an input to match empirical or analytical descriptions. As a result, the boundary slip observed from these LBM simulations is more phenomenal than physical as those from other methods, such as numerical solutions of the Boltzmann equation and the direct simulation Monte Carlo (DSMC) method. This fails to demonstrate the physical kinetic nature of LBM, which has been claimed a distinguishing feature of LBM than other CFD methods. Possible remedies to improve this drawback could be to consider high-order terms in the Chapman–Enskog expansion and to use more complicated lattice structures (Verhaeghe et al. 2009; Shan et al. 2006; Zhang et al. 2006). Further discussion can be found in a recent review (Reese and Zhang 2009).

5.2 Multiphase flows and surface effects

Multiphase fluids, such as droplets and bubbles, are commonly found in recent microfluidic applications, such as biotech lab-on-a-chips (Madou et al. 2006; Mark et al. 2009; Haber 2006), micro-electro-mechanical systems (MEMS) (Fair et al. 2007), fuel cells (Larminie and Dicks 2003), and micro heat exchangers (Hetsroni et al. 2009). In these microfluidic systems, the fluid is usually in contact with solid surfaces, either in microchannels or over patterned surfaces. Therefore, surface effects, especially the surface wettability, become significant due to the large surface-to-volume ratio (Darhuber and Troian 2005; Teh et al. 2008). The physical origin of surface wettability, usually represented by the contact angle of a liquid droplet on a surface, is the microscopic interaction between the fluid and the solid molecules.

LBM has been well accepted as an attractive choice in simulating multiphase flows. Unlike some other CFD methods, such as the VOF and level set methods, LBM algorithms for multiphase/multicomponent flows are uniform over the entire simulation domain, and no special treatment or attention is required for the deformable fluid–fluid interfaces. The phase field and interfaces are obtained from the density or index distributions. Numerous simulations have been reported for various multiphase situations, including bubble dynamics (Sankaranarayanan et al. 1999; Inamuro and Ogata 2004), droplet breakup and collision (Inamuro et al. 2004b; Chiappini et al. 2009), and interfacial instability (Shan 1997; He et al. 1999).

With the development of LBM multiphase/multicomponent models, it has been noticed that different contact angles can be easily obtained by adjusting some surface parameters. For example, D'Ortona et al. (1995) have studied the contact angle change with the wall composition of *red* and *blue* fluid particles, while the fluid was modeled as a collection of *red* and blue fluid particles with the chromodynamic model (Gunstensen et al. 1991). Clearly, this was only a conceptual or phenomenal representation of the surface. For the Shan–Chen interparticle potential model, similar to the fluid–fluid interaction, a solid–fluid interaction force between the fluid and surface is introduced to generate different contact angles (Martys and Chen 1996; Raiskinmaki et al. 2000, 2002). An attractive force is required for wetting surfaces (contact angle less than 90°), and a repulsive force will result in a nonwetting surface (contact angle larger than 90°), and the observed contact angle depends on the interaction strength. Different treatments in the free energy model can be found in the literature. Originally, similar to that in the Shan–Chen model, attractive or repulsive surface forces were utilized to simulate wetting or nonwetting surfaces (Swift et al. 1995). Later, the Cohn surface free energy has been frequently adopted, and the surface wettability is actually controlled by the normal gradient near the surface (Briant et al. 2002; Briant and Yeomans 2004).

It has been noticed that, in these surface wettability modeling methods, a neutral wettability with contact angle of 90° is typically associated with a zero controlling parameter (fluid–solid interaction or surface energy). Different signs (positive or negative) of this controlling parameter are required to model wetting and nonwetting surfaces. This is also true for other LBM multiphase models (Chang and Alexander 2006). However, physically there is no such a clear boundary for surface wettability, as demonstrated by experimental observations (Gao and McCarthy 2008) and MD simulations (Nijmeijer et al. 1990; Bertrand et al. 2009). This point has been addressed in the mean field free energy model (Zhang et al. 2004). Here different contact angles, from 0 to 180°, can be achieved by tuning the fluid–solid *attraction* strength: strong attraction for wetting and weak attraction for nonwetting surfaces (Fig. 6). Unlike previous models, no repulsion was necessary to model nonwetting surfaces. This demonstrated that the mean-field free energy model provides a better representation of solid–fluid interaction and could be useful for simulating relevant microscopic interfacial processes.

More complicated situations involving surface wettability have also been extensively simulated using various LBM models. Examples include dynamic wetting (D'Ortona et al.

1995; Zhang and Kwok 2004b; Briant et al. 2002; Briant and Yeomans 2004), capillary filling (Raiskinmaki et al. 2002; Wolf et al. 2010; Kusumaatmaja et al. 2008; Chibbaro et al. 2009a; Diotallevi et al. 2008, 2009a, b), contact angles and droplet behaviors on patterned (Zhang et al. 2009b; Kusumaatmaja et al. 2006; Chang and Alexander 2006), heterogeneous (Iwahara et al. 2003; Zhang and Kwok 2005b; Dupuis and Yeomans 2004), and rough (Raiskinmaki et al. 2000; Zhang and Kwok 2006a, 2010; Hyvaluoma et al. 2007) surfaces. Recently, electrowetting, the increase of contact angle under an applied electrical potential across the liquid and surface, has also been simulated, using the Shan–Chen interparticle potential model (Li and Fang 2009) or the free energy model (Aminfar and Mohammadpourfard 2009). The wettability controlling parameter, the solid–fluid interaction or the surface energy, is related to the applied voltage (Li and Fang 2009) or the electrical potential field (Aminfar and Mohammadpourfard 2009). However, these studies did not reflect the underlying mechanism, such as ion accumulation and electrical force near the solid–liquid interface and contact point and how they affect the contact angle (Mugele and Baret 2005). A possible approach to incorporate such underlying physics is to consider both the electric field and the ion concentration distributions, as done in previous LBM studies of electro-osmotic flows (Wang et al. 2006) and droplet deformation in electric field (Zhang and Kwok 2005a).

Another major application of multiphase LBM models is to simulate droplet dynamics in microfluidic devices (e.g., microchannels) for their practical importance in biochemical and biomedical analyses (Lin et al. 2008; Fair 2007). A controllable approach to generate desirable droplet sizes is crucial for the downstream processes, and various methods have been proposed (Lin et al. 2008; Hallmark et al. 2009; Liu and Zhang 2009; Wu et al. 2009; Mo and Kwok 2006). LBM provides an efficient method to simulate the droplet formation by considering important factors such as flow rate, surface tension, and wettability (Liu and Zhang 2009; van der Graaf et al. 2006; Gupta et al. 2009; Dupin et al. 2006). As an example, Fig. 7 displays the droplet formation process at a T junction in a microchannel (van der Graaf et al. 2006). Also, recently Liu and Zhang (2009) conducted extensive simulations to examine influences of various parameters involved in the droplet formation process, including capillary number, flow rate, viscosity, and wettability.

5.3 Solid–liquid interfacial slip

The no-slip boundary condition has been typically assumed in traditional fluid mechanics. The boundary slip in microscopic gaseous flows discussed in Sect. 5.1 is due to the low Knudsen number, at which the kinetic nature of gas molecules becomes apparent. For microscopic liquid flows, boundary slip has also been well observed with various experimental technologies (Tretheway and Meinhart 2002; Zhu and Granick 2002). The slip magnitude is usually characterized by the slip length, i.e., the ratio of the slip velocity to the shear rate at the boundary (Yang and Kwok 2003). Experimental and MD studies have revealed, in general, a correlation between the solid–liquid interfacial slip and the surface wettability: large slip is typically observed at hydrophobic surfaces with high contact angles (Barrat and Bocquet 1999; Voronov et al. 2007). This is due to the fact that interfacial slip and contact angle are both macroscopic exhibitions of their common origin—the microscopic solid–fluid interaction (Barrat and Bocquet 1999; Voronov et al. 2007). In traditional numerical methods, the boundary slip is usually imposed as a boundary condition specified by, for example, the Navier approximation (Yang and Kwok 2003).

The first LBM attempt to simulate the solid–liquid interfacial slip was conducted by Zhu et al. (2005). To generate the boundary slip in a microchannel, two different approaches have been adopted: the general LBM algorithm with a combined reflection and bounce-back boundary treatment (as those discussed in Sect. 5.1 for microscopic gaseous flows) and the Shan–Chen multicomponent model with an exponentially decaying repulsive force. Meanwhile, Zhang and Kwok (2004a) studied a similar system but with the mean field free energy model. The authors carefully set the relaxation parameter $\tau = 1$ to eliminate the artificial slip velocity from the bounce-back scheme as analyzed by He et al. (1997). Similar to the contact angle, the calculated slip length exhibits a decreasing trend with the solid–fluid attraction strength (Fig. 6). High contact angles and large slip length were obtained with weak solid–fluid attraction, and vise versa. Again this is in consistence with experimental and MD investigations, and further demonstrates that the mean field free energy LBM model possesses a realistic representation of the crucial solid–fluid interaction. Later, other LBM models, such as the Shan–Chen interparticle potential model, has also been

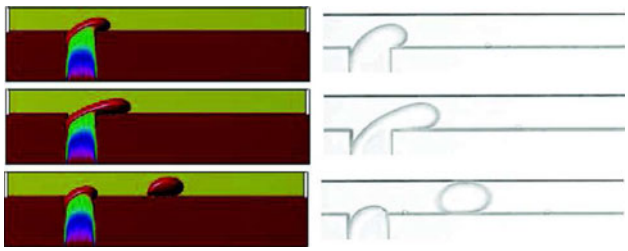

Fig. 7 Snapshots of LBM simulation (*left*) and experiment (*right*) of droplet formation at a T junction. Note the simulation and experimental pictures were displayed with different time intervals. Reprinted with permission from van der Graaf et al. (2006). Copyright 2006 American Chemical Society

employed to examine this phenomenon in more details (Benzi et al. 2006b; Harting et al. 2006).

5.4 Electrokinetic flows and electrohydrodynamic droplet deformation

A solid surface, when brought in contact with an electrolyte solution, including water, usually becomes charged due to ion absorption or surface molecule dissociation (Masliyah and Bhattacharjee 2006). A direct consequence of such a charged surface is that the ions in the electrolyte solution will then be redistributed, resulting in a higher concentration of counter-ions and a lower concentration of co-ions near the surface when compared with those in the bulk solution. The ion concentration and associated electric potential distributions in the vicinity of the surface is usually described by the well-known electrical double layer (EDL) model (Li 2004). This is the basis of several important electrokinetic phenomena in microfluidics, such as electroosmosis, electro-viscosity, stream current, stream potential, and Joule heating (Li 2004).

First LBM simulations of microchannel flows with electrokinetic effects considered were conducted by Li and Kwok (2003). Here, the equilibrium density distribution in the general LBGK algorithm was modified to incorporate the effect of the electrical potential due to the surface charge; and the electrical potential distribution was described by the analytical solution of the Poisson–Boltzmann equation with the Debye–Huckel approximation (Li and Kwok 2003). Simulated Reynolds numbers were compared with experimental measurements for various situations and good agreement was obtained. This method was also extended to include the ion exclusion volume effect near the surface (Li and Kwok 2004). In addition, Tian et al. (2005; Tian and Kwok 2005) employed this model and investigated the electroosmotic flows in microchannels with nonuniform surface potentials.

On the other hand, the electrical effects can be naturally implemented into the general LBM algorithm as an external force, with the electrical field and ion concentration distributions obtained numerically from suitable numerical schemes, including the LBM-like algorithms (Melchionna and Succi 2004; Hlushkou et al. 2004, 2005; Tang et al. 2007a; Chai and Shi 2007; Wang et al. 2006; Guo et al. 2005; Wang and Chen 2007). Interestingly, Yan et al. (2007) have studied the electroosmotic flow near an earthworm body surface when the earthworm moves in moist soil. Simulations show that moving vortices, which likely contribute to antisoil adhesion, can be formed near the earthworm body from the nonuniform and variational electrical force.

Moreover, other effects associated with microscopic flows, such as the Joule heating (Guo et al. 2005; Shi et al. 2008b; Chai et al. 2007), convection-diffusion (Kang et al. 2008; Wang et al. 2005), surface roughness (Wang et al. 2007c; Wang and Kang 2009), and solid–liquid interfacial slip (Fu et al. 2007), can also be considered. Active topics of these simulations also include microflows in porous media (Park et al. 2007; Hlushkou et al. 2005; Guo and Zhao 2002) and mixing efficiency improvement in microchannels with nonuniform surface potential (Tian et al. 2005; Kang et al. 2008; Wang and Kang 2010a) (Fig. 8). Energy conversion by means of electrokinetic flows in microchannels (Yang et al. 2003) have also been simulated (Wang and Kang 2010b). In addition, multiphase LBM models have also been utilized to simulate the electrohydrodynamic deformation of droplets suspending in electric field (Zhang and Kwok 2005a; Huang et al. 2007). The simulated droplet deformation and flow field were found in good agreement with other theoretical and experimental studies.

5.5 Magnetohydrodynamic flows

Magnetic forces have been extensively involved in various microfluidic applications, including micropumps, microvalves, stirrers, and manipulating magnetic particles in microflows (Qian and Bau 2009; Pamme 2006; Gijs 2004).

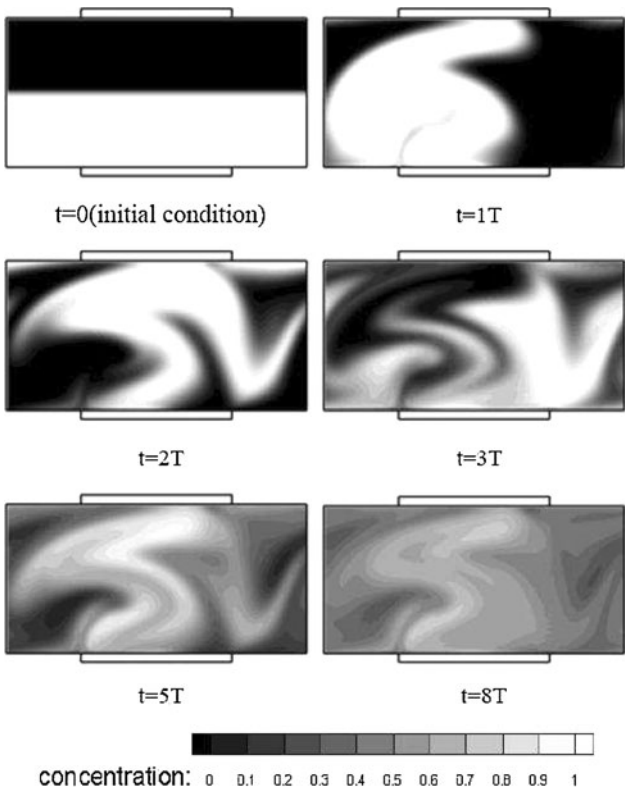

Fig. 8 Simulated concentration patterns under an applied electrical field in a microchannel with heterogeneous surface potential (Kang et al. 2008). Reprinted with kind permission of Springer Science and Business Media

With the LBM models for magnetohydrodynamics (MHD) available (Dellar 2002; Breyiannis and Valougeorgis 2004), several MHD simulations of microfluidic systems have been reported. For example, Sofonea et al. (2002; Sofonea and Fruh 2001) had simulated the deformation of magnetic fluid drops (or gas bubbles in magnetic fluids) and the normal field instability of magnetic fluids under the action of an external magnetic field. Similar phenomena has also been investigated recently by Clime et al. (2009) had simulated the splitting process of a magnetic droplet with a hydrophilic magnetic plug inside in electrowetting-on-dielectric devices, and the simulation results had been compared with experimental observations with excellent agreement. On the hand, the dynamics of paramagnetic particles under rotating magnetic fields in fluid has also been studied (Calhoun et al. 2006; Krishnamurthy et al. 2008) for its potential application in microfluidic mixing. Another interesting area that LBM methods could be useful is the electro-magneto-hydrodynamic-based microfluidic devices (Qian and Bau 2009), which involve electrical field, magnetic field, fluid mechanics, ion diffusion-convection, as well as possible heat transfer. However, so far no LBM simulations of these complex but important processes have been reported yet.

5.6 Microflows in porous media

Another major attractiveness of LBM is the relative easiness in dealing with complex boundary geometry due to its particulate dynamics. This merit is best demonstrated by simulations of flows through porous materials, where microscopic porous structure and even surface wettability can be considered explicitly. Successful applications can be traced back to the early years of LBM development in early 1990s. For example, in 1993 Gunstensen and Rothman (1993) investigated immiscible two-phase flows in a 3D microscopic model of a porous medium using the chromodynamic multiphase model (Gunstensen et al. 1991). It was observed that the conventional linear Darcy law is applicable only for high forcing. However, at low levels of forcing, the microscopic capillary effect becomes important and the flow-force relation becomes nonlinear. Similarly, Martys and Chen (1996) had applied the interparticle potential model to a digitalized 3D porous structure of sandstone. In addition, Maier and Bernard (2010) have also examined the numerical accuracy of porous flows with different boundary treatments. Recently, a wave of interest in porous flows has been seen due to their particular application in fuel cells (Larminie and Dicks 2003). In such situations, a detailed description of fluid mass transport processes is necessary to study the effects of porous structures and surface wettability. Joshi et al. (2007, 2010) had simulated the multi-component gas diffusion phenomenon in a solid oxide fuel cell anode. In addition, electrochemical reactions in the anode layer can also be considered (Asinari et al. 2007; Suzue et al. 2008; Chiu et al. 2009). Multiphase flows in polymer electrolyte membrane fuel cells have also been studied extensively using multiphase LBM models with the surface wettability effect considered (Niu et al. 2007; Sinha et al. 2007; Koido et al. 2008; Tabe et al. 2009; Tomiyasu and Inamuro 2009) (Fig. 9). Other applications of porous flows have also been explored, for example, in underground water resources (Kang et al. 2006; Porter et al. 2009), fabric materials (Ramaswamy et al. 2004; Belov et al. 2004), and biological and biomedical materials (Zeiser et al. 2008; Porter et al. 2005). Electroosmosic flows through porous materials have also been examined (Wang and Chen 2007; Wang et al. 2007b).

5.7 Biological microfluidics

LBM has attracted increasing interests in simulating biological flows during its advances in the past decades. Both blood flows in vessels (Fang et al. 1998; Krafczyk et al. 1998; Ouared and Chopard 2005; Boyd and Buick 2008) and air flows in lung (Freitas and Schroder 2008) have been investigated. In vessels larger than 200 μm, blood flows can be accurately modeled as a homogeneous fluid. However, in smaller microvessels and capillaries, blood has to be considered as a suspension of discrete blood cells, since their sizes are now comparable to the microvessel/capillary diameter (Popel and Johnson 2005).

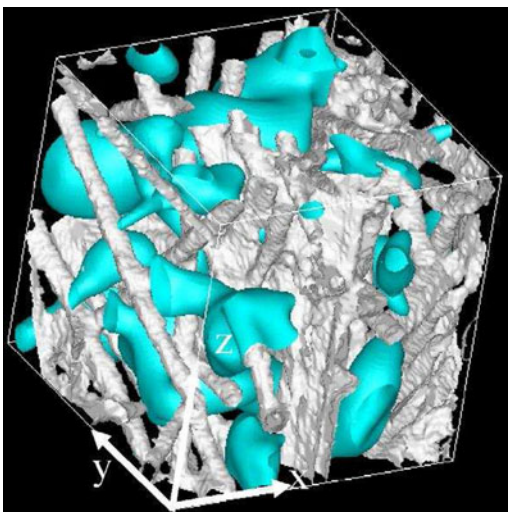

Fig. 9 Fibrous structure and water distribution in a modeled gas diffusion layer of proton exchange membrane fuel cells. The flow direction is in the *x* direction. Reprinted from Koido et al. (2008) with permission from Elsevier

To address the particulate nature of microscopic blood flows, Migliorini et al. (2002) have developed a LBM model with red blood cells (RBCs) and white blood cells (WBCs) represented as rigid particles. This model thereafter has been applied to various situations, including WBC dynamics, microscopic hemorheology, plasma leakage, and blood flows in modeled vessel networks (Munn and Dupin 2008). On the other hand, Li et al. (2004) have examined suspension flows through a stenotic artery, where RBCs were modeled as circular rigid particles.

However, these studies utilized rigid particles to model the highly deformable RBCs. It is well known that RBCs can deform greatly and pass through capillaries even smaller than the RBC size, and the membrane deformability is a determinant factor in blood hemodynamics and hemorheology (Popel and Johnson 2005; Stoltz et al. 1999). In addition, RBCs can also aggregate together and form one-dimensional stacks-of-coins-like rouleaux or three-dimensional aggregates (Popel and Johnson 2005; Stoltz et al. 1999). RBC aggregation can affect in vivo hemodynamic behaviors, especial in low shear flow regions in the venules, and increased aggregation is often observed in various diseases and pathological situations, such as diabetes, heart diseases, malaria, and inflammation (Baskurt and Meiselman 2007). To provide a better representation of RBC flows in microvessels, Zhang et al. (2007) have developed an immersed boundary lattice Boltzmann model (IB-LBM), where RBCs were modeled as liquid capsules enclosed with deformable membrane using IBM (Peskin 1977). The important aggregation effect has also been incorporated using a Morse potential to describe the cell–cell attraction. With this algorithm, the authors have examined RBC aggregation and dissociation in shear flow (Zhang et al. 2008) and effects of RBC membrane deformability and aggregation on blood flows (Zhang et al. 2007, 2009a). Several hemodynamic and hemorheological characteristics have been well reproduced, such as the tumbling-rotating and tank-treading motions of a RBC in shear flow, RBC migration and cell-free layer development, blunt velocity profiles, and the Fahraeus and Fahraeus-Lindqvist effects (Zhang et al. 2010). For the importance of shear stress in microcirculations (Ando and Yamamoto 2009; Reneman et al. 2006), recently, this method has been applied to study the relationship between RBC motion and the induced shear stress variation in microvessels (Xiong and Zhang 2010a).

Three-dimensional models have also been developed to simulate RBC flows more accurately. Dupin et al. (2007) have modeled a deformable RBC as a spring network, and constraints on membrane area, cell volume, local curvature, and local primary stresses can be implemented as nodal forces. The fluid–membrane interaction was accomplished using a method similar to the immersed boundary treatment. Simulated RBC deformation has been compared with optical tweezers measurements and good agreement was observed. Furthermore, a suspension consisting 200 deformable RBCs flowing through a rectangular channel was simulated and significant pressure variation has been reported (Fig. 10). On the other hand, Sui et al. (2008) adopted a finite element representation for deformable membrane and a strain energy function was utilized to describe the membrane mechanics. Again, the fluid flow was simulated with LBM and the fluid–membrane interaction was implemented via IBM. Deformation of capsules with various initial resting shapes under shear flows has been studied, and the tank-treading, swinging, and tumbling motions of the capsules have been reproduced (Sui et al. 2008). More recently, MacMeccan et al. (2009) proposed another finite-element lattice Boltzmann scheme; however, the fluid–membrane interaction was implemented by treating the membrane as a moving boundary using the Ladd modified bounce-back method (Ladd 1994b). This fluid–membrane coupling method needs to solve the nodal displacement and velocity from the hydrodynamic force exerted on the membrane surfaces, while the IBM directly calculates the membrane nodal force from membrane deformation. In addition, white blood cell transport has also been studied with the microscopic blood flow modeled as a suspension of blood cells (Migliorini et al. 2002; Munn and Dupin 2008) or a continuum fluid (Artoli et al. 2007).

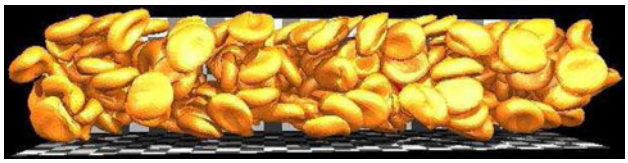

Fig. 10 Simulation of 200 RBCs flowing in a 3D rectangular microchannel. Reprinted with permission from Dupin et al. (2007). Copyright 2007 by the American Physical Society

6 Conclusions

We have summarized LBM models for fluid flows and other processes such as heat transfer, diffusion, and electric field. Typical strategies of force implementation, initial condition, and boundary condition in LBM practices have been introduced. We also reviewed extensive LBM applications in various microfluidic systems. These simulations demonstrate that LBM is an efficient and useful approach for computational microfluidics for its physical representation of microscopic interactions and convenience in modeling complex boundaries.

Although about 300 publications have been referred in this review, the coverage is definitely not complete due to the large amount of literature and diverse interests in LBM and microfluidics. Many interesting applications have not

been discussed, such as particulate flows and colloidal suspensions (Ladd 1994a; Feng and Michaelides 2004; Heemels et al. 2000; Joshi and Sun 2009), macromolecule dynamics in flow field (Fyta et al. 2006; Giupponi et al. 2007; Chen et al. 2007), and ion–particle interaction in electrolyte solutions (Chatterji and Horbach 2007; Lobaskin et al. 2004). On the other hand, physical principles and mathematical analysis are intensively involved in the development of various LBM models. However, this article was composed from a practical point of view for researchers in computational microfluidics, and the theoretical aspects were not addressed in details. Nevertheless, knowledge of these involved theories might be necessary to better understand the strength and limit of LBM in simulating microfluidic systems, and interested readers can refer to the relevant literature.

At last, it should be mentioned that, in spite of the attractiveness and successful applications of LBM, as any other numerical methods, it has certain limits. First of all, LBM is a mesoscopic approach and the detailed microscopic features, such as the exact molecular structures and intermolecular interactions cannot be represented explicitly. Also for gaseous microflows with higher Knudsen numbers, the LBM algorithm may not be suitable even for the bulk flow region. Actually, a recent comparative study of capillary filling in rough channels of 0.8-μm wide channels indicates that, in the vicinity of the critical angle, the motion of the liquid front exhibits a strong sensitivity to molecular fluctuations that cannot be accounted for by a standard (nonfluctuating) LB methods (Chibbaro et al. 2009b). Therefore, in such situations, other molecular simulation techniques, including MD (Dimitrov et al. 2007; Cannon and Hess 2010) and DSMC (Roohi et al. 2009; Xu and Li 2004), should be utilized. In addition, in some situations, for example, multiphase flows with large density difference and/or with heat transfer involved, other multiphase models such as VOF (Scardovelli and Zaleski 1999), the level-set method (Sethian and Smereka 2003), or other diffuse interface method (Anderson et al. 1998), could also be considered.

Acknowledgments This study was supported by the Natural Sciences and Engineering Research Council of Canada (NSERC) and the Laurentian University Research Fund (LURF). The author acknowledges the helpful discussion with Prof. Donald E. Sullivan at University of Guelph. The author also thanks the anonymous reviewers for their critical comments and constructive suggestions.

References

Abe T (1997) Derivation of the lattice Boltzmann method by means of the descrete ordinate method for the Boltzmann equation. J Comput Phys 131:241–246

Agrawal A, Djenidi L, Antonia RA (2005) Simulation of gas flow in microchannels with a sudden expansion or contraction. J Fluid Mech 530:135–144

Aidun CK, Clausen JR (2010) Lattice-Boltzmann method for complex flows. Ann Rev Fluid Mech 42:439–472

Aidun CK, Lu Y, Ding E (1998) Direct analysis of particulate suspensions with inertia using the discrete Boltzmann equation. J Fluid Mech 373:287–311

Al-Zoubi A, Brenner G (2004) Comparative study of thermal flows with different finite volume and lattice Boltzmann schemes. Int J Modern Phys C 15:307–319

Alexanders F, Chen S, Sterling J (1993) Lattice Boltzmann thermohydrodynamics. Phys Rev E 47:R2249–R2252

Aminfar H, Mohammadpourfard M (2009) Lattice Boltzmann method for electrowetting modeling and simulation. Comput Methods Appl Mech Eng 198:3852–3868

Anderson DM, McFadden GB, Wheeler AA (1998) Diffuse-interface methods in fluid mechanics. Ann Rev Fluid Mech 30:139–165

Ando J, Yamamoto K (2009) Vascular mechanobiology: endothelial cell responses of fluid shear stress. Circulation J 73:1983–992

Ansumali S, Karlin IV (2002) Kinetic boundary conditions in the lattice Boltzmann method. Phys Rev E 66:026311

Ansumali S, Karlin IV, Frouzakis CE, Boulouchos KB (2006) Entropic lattice Boltzmann method for microflows. Phys A 359:289–305

Artoli AM, Sequeira A, Silva-Herdade AS, Saldanha C (2007) Leukocytes rolling and recruitment by endothelial cells: hemorheological experiments and numerical simulations. J Biomech 40:3493–3502

Asinari P, Quaglia MC, von Spakovsky MR, Kasula BV (2007) Direct numerical calculation of the kinematic tortuosity of reactive mixture flow in the anode layer of solid oxide fuel cells by the lattice Boltzmann method. J Power Sour 170:359–375

Bao J, Yuan P, Schaefer L (2008) A mass conserving boundary condition for the lattice Boltzmann equation method. J Comput Phys 227:8472–8487

Barrat JL, Bocquet L (1999) Large slip effect at a nonwetting fluid-solid interface. Phys Rev Lett 82:4671–4674

Baskurt O, Meiselman H (2007) Hemodynamic effects of red blood cell aggregation. Indian J Exp Biol 45:25–31

Belov EB, Lomov SV, Verpoest I, Peters T, Roose D, Parnas RS, Hoes K, Sol H (2004) Modelling of permeability of textile reinforcements: lattice Boltzmann method. Compos Sci Technol 64:1069–1080

Benzi R, Succi S, Gassola MV (1992) The lattice Boltzmann-equation—theory and applications. Phys Rep Rev Sect Phys Lett 222:145–197

Benzi R, Biferale L, Sbragaglia M, Succi S, Toschi F (2006a) Mesoscopic modeling of a two-phase flow in the presence of boundaries: the contact angle. Phys Rev E 74:021509

Benzi R, Biferale L, Sbragaglia M, Succi S, Toschi F (2006b) Mesoscopic two-phase model for describing apparent slip in micro-channel flows. Europhys Lett 74:651–657

Benzi R, Sbragaglia M, Succi S, Bernaschi M, Chibbaro S (2009) Mesoscopic lattice Boltzmann modeling of soft-glassy systems: theory and simulations. J Chem Phys 131:104903

Bertrand E, Blake TD, De Coninck J (2009) Influence of solid-liquid interactions on dynamic wetting: a molecular dynamics study. J Phys Condens Matter 21:464124

Beskok A, Karniadakis GE, Trimmer W (1996) Rarefaction and compressibility effects in gas microflows. J Fluid Eng 118:448–456

Besold G, Vattulainen I, Karttunen M, Polson JM (2000) Towards better integrators for dissipative particle dynamics simulations. Phys Rev E 62:R7611–R7614

Bhatnagar P, Gross E, Krook M (1954) A model for collisional processes in gases I: small amplitude processes in charged and neutral one-component system. Phys Rev 94:511–525
Boyd J, Buick JM (2008) Three-dimensional modelling of the human carotid artery using the lattice Boltzmann method: I. model and velocity analysis. Phys Med Biol 53:5767–5779
Breyiannis G, Valougeorgis D (2004) Lattice kinetic simulations in three-dimensional magnetohydrodynamics. Phys Rev E 69:065702
Briant AJ, Yeomans JM (2004) Lattice Boltzmann simulations of contact line motion. II. Binary fluids. Phys Rev E 69:031603
Briant AJ, Papatzacos P, Yeomans JM (2002) Lattice Boltzmann simulations of contact line motion in a liquid-gas system. Philos Trans Roy Soc Lond A 360:485–495
Briant A, Wagner A, Yeomans J (2004) Lattice Boltzmann simulations of contact line motion. I: liquid-gas systems. Phys Rev E 69:031602
Buick JM (1997) Lattice Boltzmann methods in interfacial wave modelling. PhD thesis, University of Edinburgh
Buick JM, Greated CA (2000) Gravity in a lattice Boltzmann model. Phys Rev E 61:5307–5320
Cahn J, Hilliard J (1958) Free energy of a nonuniform system i: interfacial free energy. J Chem Phys 28:258–267
Calhoun R, Yadav A, Phelan P, Vuppu A, Garcia A, Hayes M (2006) Paramagnetic particles and mixing in micro-scale flows. Lab Chip 6:247–257
Cannon J, Hess O (2010) Fundamental dynamics of flow through carbon nanotube membranes. Microfluid Nanofluid 8:21–31
Chai Z, Shi B (2007) Simulation of electro-osmotic flow in microchannel with lattice Boltzmann method. Phys Lett A 364:183–188
Chai Z, Shi B, Zheng L (2007) Lattice Boltzmann simulation of viscous dissipation in electro-osmotic flow in microchannels. Int J Modern Phys C 18:1119–1131
Chai Z, Guo Z, Zheng L, Shi B (2008) Lattice Boltzmann simulation of surface roughness effect on gaseous flow in a microchannel. J Appl Phys 104:014902
Chang Q, Alexander J (2006) Analysis of single droplet dynamics on striped surface domains using a lattice Boltzmann method. Microfluid Nanofluid 2:309–326
Chatterjee D (2009) An enthalpy-based thermal lattice Boltzmann model for non-isothermal systems. EPL 86:14004
Chatterji A, Horbach J (2007) Electrophoretic properties of highly charged colloids: a hybrid molecular dynamics/lattice Boltzmann simulation study. J Chem Phys 126:064907
Chen Y (1994) Thermal lattice Bhatnagar–Gross–Krook model without nonlinear deviations in macrodynamic equations. Phys Rev E 50:2776
Chen S, Doolen GD (1998) Lattice Boltzmann method for fluid flows. Ann Rev Fluid Mech 30:329–364
Chen X, Shi B (2005) A new lattice Boltzmann model for incompressible magnetohydrodynamics. Chin Phys 14:1398–1406
Chen S, Chen H, Martnez D, Matthaeus W (1991) Lattice Boltzmann model for simulation of magnetohydrodynamics. Phys Rev Lett 67:3776–3779
Chen Y, Ma H, Graham MD, de Pablo JJ (2007) Modeling DNA in confinement: a comparison between the brownian dynamics and lattice Boltzmann method. Macromolecule 40:5978–5984
Chiappini D, Bella G, Succi S, Ubertini S (2009) Applications of finite-difference lattice Boltzmann method to breakup and coalescence in multiphase flows. Int J Modern Phys C 20:1803–1816
Chibbaro S, Biferale L, Binder K, Dimitrov D, Diotallevi F, Milchev A, Succi S (2009a) Hydrokinetic simulations of nanoscopic precursor films in rough channels. J Stat Mech Theory Exp. doi: 10.1088/1742-5468/2009/06/P06007
Chibbaro S, Costa E, Dimitrov DI, Diotallevi F, Milchev A, Palmieri D, Pontrelli G, Succi S (2009b) Capillary filling in microchannels with wall corrugations: a comparative study of the Concus-Finn criterion by continuum, kinetic, and atomistic approaches. Langmuir 25:12653–12660
Chiu WKS, Joshi AS, Grew KN (2009) Lattice Boltzmann model for multi-component mass transfer in a solid oxide fuel cell anode with heterogeneous internal reformation and electrochemistry. Eur Phys J Special Top 171:159–165
Clime L, Brassard D, Veres T (2009) Numerical modeling of the splitting of magnetic droplets by multiphase lattice Boltzmann equation. J Appl Phys 105:07B517
Darhuber AA, Troian SM (2005) Principles of microfluidic actuation by modulation of surface stresses. Ann Rev Fluid Mech 37:425–455
Dawson S, Chen S, Doolen G (1993) Lattice Boltzmann computations for reaction-diffusion equations. J Chem Phys 98:1514–1523
de Jong J, Lammertink RGH, Wessling M (2006) Membranes and microfluidics: a review. Lab Chip 6:1125–1139
Dellar PJ (2002) Lattice kinetic schemes for magnetohydrodynamics. J Comput Phys 179:95–126
d'Humieres D, Ginzburg I, Krafczyk M, Lallemand P, Luo L (2002) Multiple-relaxation-time lattice Boltzmann models in three-dimensions. Philos Trans Roy Soc Lond A 360:437–451
Dimitrov DI, Milchev A, Binder K (2007) Capillary rise in nanopores: molecular dynamics evidence for the Lucas-Washburn equation. Phys Rev Lett 99:054501
Diotallevi F, Biferale L, Chibbaro S, Puglisi A, Succi S (2008) Front pinning in capillary filling of chemically coated channels. Phys Rev E 78:036305
Diotallevi F, Biferale L, Chibbaro S, Lamura A, Pontrelli G, Sbragaglia M, Succi S, Toschi F (2009a) Capillary filling using lattice Boltzmann equations: the case of multi-phase flows. Eur Phys J Special Top 166:111–116
Diotallevi F, Biferale L, Chibbaro S, Pontrelli G, Toschi F, Succi S (2009b) Lattice Boltzmann simulations of capillary filling: finite vapour density effects. Eur Phys J Special Top 171:237–243
D'Orazio A, Succi S (2004) Simulating two-dimensional thermal channel flows by means of a lattice Boltzmann method with new boundary conditions. Futur Gener Comput Syst 20:935–944
D'Ortona U, Salin D, Cieplak M, Rybka RB, Banavar JR (1995) 2-color nonlinear Boltzmann cellular-automata—surface-tension and wetting. Phys Rev E 51:3718–3728
Dunweg B, Ladd AJC (2009) Lattice Boltzmann simulations of soft matter systems. Adv Polym Sci 221:89–166
Dupin MM, Halliday I, Care CM (2006) Simulation of a microfluidic flow-focusing device. Phys Rev E 73:055701
Dupin MM, Halliday I, Care CM, Alboul L, Munn LL (2007) Modeling the flow of dense suspensions of deformable particles in three dimensions. Phys Rev E 75:066707
Dupuis A, Yeomans JM (2004) Lattice Boltzmann modelling of droplets on chemically heterogeneous surfaces. Futur Gener Comput Syst 20:993–1001
Dupuis A, Chatelain P, Koumoutsakos P (2008) An immersed boundary-lattice-Boltzmann method for the simulation of the flow past an impulsively started cylinder. J Comput Phys 227:4486–4498
Fair RB (2007) Digital microfluidics: is a true lab-on-a-chip possible? Microfluid Nanofluid 3:245–281
Fair RB, Khlystov A, Tailor TD, Ivanov V, Evans RD, Griffin PB, Srinivasan V, Pollack V, Zhou J (2007) Chemical and biological applications of digital-microfluidic devices. IEEE Des Test Comput 24:10–24

Fan L, Fang H, Lin Z (2001) Simulation of contact line dynamics in a two-dimensional capillary tube by the lattice Boltzmann model. Phys Rev E 63:051603

Fang H, Lin Z, Wang Z (1998) Lattice Boltzmann simulation of viscous fluid systems with elastic boundaries. Phys Rev E 57:R25–R28

Feng Z, Michaelides EE (2004) The immersed boundary-lattice Boltzmann method for solving fluid-particles interaction problems. J Comput Phys 195:602–628

Filipovic N, Ivanovic M, Kojic M (2009) A comparative numerical study between dissipative particle dynamics and smoothed particle hydrodynamics when applied to simple unsteady flows in microfluidics. Microfluid Nanofluid 7:227–235

Filippova O, Hanel D (1998) Grid refinement for lattice-BGK models. J Comput Phys 147:219–228

Fisk S, Widom B (1969) Structure and free energy of interface between fluid phases in equilibrium near critical point. J Chem Phys 50:3219–3227

Freed DM (1998) Lattice Boltzmann method for macroscopic porous media modeling. Int J Modern Phys C 9:1491–1503

Freitas RK, Schroder W (2008) Numerical investigation of the three-dimensional flow in a human lung model. J Biomech 41:2446–2457

Freudiger S, Hegewald J, Krafczyk M (2008) A parallelisation concept for a multi-physics lattice Boltzmann prototype based on hierarchical grids. Prog Comput Fluid Dyn 8:168–178

Fu X, Li B, Zhang J, Tian F, Kwok DY (2007) Electrokinetic slip flow of microfluidics in terms of streaming potential by a lattice Boltzmann method: A bottom-up approach. Int J Modern Phys C 18:693–700

Fyta MG, Melchionna S, Kaxiras E, Succi S (2006) Multiscale coupling of molecular dynamics and hydrodynamics: Application to DNA translocation through a nanopore. Multiscale Model Simul 5:1156–1173

Gad-el-Hak M (1999) The fluid mechanics of microdevices—the Freeman scholar lecture. J Fluids Eng 121:5–33

Gao L, McCarthy TJ (2008) Teflon is hydrophilic: comments on definitions of hydrophobic, shear versus tensile hydrophobicity, and wettability characterization. Langmuir 24:9183–9188

Geller S, Krafczyk M, Toelke J, Turek S, Hron J (2006) Benchmark computations based on lattice-Boltzmann, finite element and finite volume methods for laminar flows. Computers and Fluids 35:888–897

Gijs MAM (2004) Magnetic bead handling on-chip: new opportunities for analytical applications. Microfluid Nanofluid 1:22–40

Ginzburg I, Steiner K (2003) Lattice Boltzmann model for free-surface flow and its application to filling process in casting. J Comput Phys 185:61–99

Giupponi G, De Fabritiis G, Coveney PV (2007) Hybrid method coupling fluctuating hydrodynamics and molecular dynamics for the simulation of macromolecules. J Chem Phys 126:154903

Gunstensen AK, Rothman RH (1993) Lattice-Boltzmann studies of immiscible 2-phase flow through porous-media. J Geophys Res Solid Earth 98:6431–6441

Gunstensen A, Rothman D, Zaleski S, Zanetti G (1991) Lattice Boltzmann model of immiscible fluids. Phys Rev A 43:4320–4327

Guo Z, Zhao T (2002) Lattice Boltzmann model for incompressible flows through porous media. Phys Rev E 66:036304

Guo Z, Zheng C (2008) Analysis of lattice Boltzmann equation for microscale gas flows: relaxation times, boundary conditions and the Knudsen layer. Int J Comput Fluid Dyn 22:465–473

Guo Z, Shi B, Wang N (1999) Fully Lagrangian and lattice Boltzmann methods for the advection-diffusion equation. J Sci Comput 14:291–300

Guo Z, Zheng C, Shi B (2002a) Discrete lattice effects on the forcing term in the lattice Boltzmann method. Phys Rev E 65:046308

Guo Z, Zheng C, Shi B (2002b) An extrapolation method for boundary conditions in lattice Boltzmann method. Phys Fluids 14:2007–2010

Guo Z, Zhao T, Shi Y (2005) A lattice Boltzmann algorithm for electro-osmotic flows in microfluidic devices. J Chem Phys 122:144907

Guo Z, Zhao T, Shi Y (2006) Physical symmetry, spatial accuracy, and relaxation time of the lattice Boltzmann equation for microgas flows. J Appl Phys 99:074903

Guo Z, Shi B, Zhao T, Zheng C (2007) Discrete effects on boundary conditions for the lattice Boltzmann equation in simulating microscale gas flows. Phys Rev E 76:056704

Guo Z, Zheng C, Shi B (2008) Lattice Boltzmann equation with multiple effective relaxation times for gaseous microscale flow. Phys Rev E 77:036707

Guo Z, Han H, Shi B, Zheng C (2009) Theory of the lattice Boltzmann equation: Lattice Boltzmann model for axisymmetric flows. Phys Rev E 79:046708

Gupta A, Murshed S, Kumar R (2009) Droplet formation and stability of flows in a microfluidic T-junction. Appl Phys Lett 94:164107

Haber C (2006) Microfluidics in commercial applications: an industry perspective. Lab Chip 6:1118–1121

Hallmark B, Parmar C, Walker D, Hornung CH, Mackley MR, Davidson JF (2009) The experimental observation and modelling of microdroplet formation within a plastic microcapillary array. Chem Eng Sci 64:4758–4764

Harting J, Kunert C, Herrmann HJ (2006) Lattice Boltzmann simulations of apparent slip in hydrophobic microchannels. Europhys Lett 75:328–334

He X, Li N (2000) Lattice Boltzmann simulation of electrochemical systems. Comput Phys Commun 129:158–166

He X, Luo L-S (1997) A priori derivation of the lattice Boltzmann equation. Phys Rev E 55:6333–6336

He X, Zou Q, Luo L, Dembo M (1997) Analytic solutions of simple flows and analysis of nonslip boundary conditions for the lattice Boltzmann BGK model. J Stat Phys 87:115–136

He X, Chen S, Doolen GD (1998) A novel thermal model for the lattice Boltzmann method in incompressible limit. J Comput Phys 146:282–300

He X, Chen S, Zhang R (1999) A lattice Boltzmann scheme for incompressible multiphase flow and its application in simulation of Rayleigh-Taylor instability. J Comput Phys 152:642–663

He X, Li N, Goldstein B (2000) Lattice Boltzmann simulation of diffusion-convection systems with surface chemical reaction. Mol Simul 25:145–156

Heemels MW, Hagen MHJ, Lowe CP (2000) Simulating solid colloidal particles using the lattice-Boltzmann method. J Comput Phys 164:48–61

Hetsroni G, Mosyak A, Pogrebnyak E, Segal Z (2009) Heat transfer of gas-liquid mixture in micro-channel heat sink. Int J Heat Mass Transf 52:3963–3971

Hlushkou D, Kandhai D, Tallarek U (2004) Coupled lattice-Boltzmann and finite-difference simulation of electroosmosis in microfluidic channels. Int J Numer Methods Fluids 46:507–532

Hlushkou S, Seidel-Morgenstern A, Tallarek U (2005) Numerical analysis of electroosmotic flow in dense regular and random arrays of impermeable, nonconducting spheres. Langmuir 21:6097–6112

Ho CM, Tai YC (1998) Micro-electro-mechanical-systems (MEMS) and fluid flows. Ann Rev Fluid Mech 30:579–612

Horbach J, Succi S (2006) Lattice Boltzmann versus molecular dynamics simulation of nanoscale hydrodynamic flows. Phys Rev Lett 96:224503

Hou S, Shan X, Zou Q, Doolen GD, Soll WE (1997) Evaluation of two lattice Boltzmann models for multiphase flows. J Comput Phys 138:695–713

Huang H, Lu X (2009) Theoretical and numerical study of axisymmetric lattice Boltzmann models. Phys Rev E 80:016701
Huang W, Li Y, Liu Q (2007) Application of the lattice Boltzmann method to electrohydrodynamics: deformation and instability of liquid drops in electrostatic fields. Chin Sci Bul 52:3319–3324
Hyvaluoma J, Koponen A, Raiskinmaki P, Timonen J (2007) Droplets on inclined rough surfaces. Eur Phys J E 23:289–293
Inamuro T, Ogata T (2004) A lattice kinetic scheme for bubble flows. Philos Trans Roy Soc Lond A 362:1735–1743
Inamuro T, Yoshino M, Inoue H, Mizuno R, Ogino F (2002) A lattice Boltzmann method for a binary miscible fluid mixture and its application to a heat-transfer problem. J Comput Phys 179:201–215
Inamuro T, Tomita R, Ogino F (2003) Lattice Boltzmann simulations of drop deformation and breakup in shear flows. Int J Modern Phys B 17:21–26
Inamuro T, Ogata T, Tajima S, Konishi N (2004a) A lattice Boltzmann method for incompressible two-phase flows with large density differences. J Comput Phys 198:628–644
Inamuro T, Tajima S, Ogino F (2004b) Lattice Boltzmann simulation of droplet collision dynamics. Int J Heat Mass Transf 47:4649–4657
Iwahara D, Shinto H, Miyahara M, Higashitani K (2003) Liquid drops on homogeneous and chemically heterogeneous surfaces: A two-dimensional lattice Boltzmann study. Langmuir 19:9086–9093
Izquierdo S, Martínez-Lera P, Fueyo N (2009) Analysis of open boundary effects in unsteady lattice Boltzmann simulations. Comput Math Appl 58:914–921
Joshi AS, Sun Y (2009) Multiphase lattice Boltzmann method for particle suspensions. Phys Rev E 79:066703
Joshi AS, Grew KN, Peracchio AA, Chiu WKS (2007) Lattice Boltzmann modeling of 2D gas transport in a solid oxide fuel cell anode. J Power Sour 164:631–638
Joshi AS, Grew KN, Izzo JR Jr., Peracchio AA, Chiu WKS (2010) Lattice Boltzmann modeling of three-dimensional, multicomponent mass diffusion in a solid oxide fuel cell anode. J Fuel Cell Sci Technol 7:011006
Kadau K, Germann TC, Lomdahl PS (2006) Molecular dynamics comes of age: 320 billion atom simulation on Bluegene/L. Int J Modern Phys C 17:1755–1761
Kang Y, Li D (2009) Electrokinetic motion of particles and cells in microchannels. Microfluid Nanofluid 6:431–460
Kang Q, Zhang D, Chen S (2002) Displacement of a two-dimensional immiscible droplet in a channel. Phys Fluids 14:3203–3214
Kang Q, Lichtner PC, Zhang D (2006) Lattice Boltzmann pore-scale model for multicomponent reactive transport in porous media. J Geophys Res Solid Earth 111:B05203
Kang J, Heo HS, Suh YK (2008) LBM simulation on mixing enhancement by the effect of heterogeneous zeta-potential in a microchannel. J Mech Sci Technol 22:1181–1191
Kaufman A, Fan Z, Petkov K (2009) Implementing the lattice Boltzmann model on commodity graphics hardware. J Stat Mech Theory Exp. doi:10.1088/1742-5468/2009/06/P06016
Kim SH, Pitsch H, Boyd ID (2008) Accuracy of higher-order lattice Boltzmann methods for microscale flows with finite Knudsen numbers. J Comput Phys 227:8655–8671
Klar A, Seaid M, Thommes G (2008) Lattice Boltzmann simulation of depth-averaged models in flow hydraulics. Int J Comput Fluid Dyn 22:507–522
Koido T, Furusawa T, Moriyama K (2008) An approach to modeling two-phase transport in the gas diffusion layer of a proton exchange membrane fuel cell. J Power Sour 175:127–136
Korner C, Thies M, Hofmann T, Thurey N, Rude U (2005) Lattice Boltzmann model for free surface flow for modeling foaming. J Stat Phys 121:179–196
Krafczyk M, Cerrolaza M, Schulz M, Rank E (1998) Analysis of 3D transient blood flow passing through an artificial aortic valve by lattice-Boltzmann methods. J Biomech 31:453–462
Krishnamurthy S, Yadav A, Phelan PE, Calhoun R, Vuppu AK, Hayes AAGMA (2008) Dynamics of rotating paramagnetic particle chains simulated by particle dynamics, stokesian dynamics and lattice Boltzmann methods. Microfluid Nanofluid 5:33–41
Kusumaatmaja H, Leopoldes J, Dupuis A, Yeomans JM (2006) Drop dynamics on chemically patterned surfaces. Europhys Lett 73:740–746
Kusumaatmaja H, Pooley CM, Girardo S, Pisignano D, Yeomans JM (2008) Capillary filling in patterned channels. Phys Rev E 77:067301
Kuznik F, Obrecht C, Rusaouen G, Roux J-J (2010) LBM based flow simulation using GPU computing processor. Comput Math Appl. doi:10.1016/j.camwa.2009.08.052
Ladd A (1994a) Numerical simulations of particulate suspensions via a discretized Boltzmann-equation. 2. Numerical results. J Fluid Mech 271:311–339
Ladd AJC (1994b) Numerical simulations of particulate suspensions via a discretized Boltzmann-equation i: theoretical foundation. J Fluid Mech 271:285–309
Ladd AJC, Verberg R (2001) Lattice-Boltzmann simulations of particle-fluid suspensions. J Stat Phys 104:1191–1251
Lai Y, Lin C, Huang J (2001) Accuracy and efficiency study of lattice Boltzmann method for steady-state flow simulations. Numer Heat Transf B 39:21–43
Lallemand P, Luo L (2000) Theory of the lattice Boltzmann method: dispersion, dissipation, isotropy, Galilean invariance, and stability. Phys Rev E 61:6546–6562
Larminie J, Dicks A (2003) Fuel cell systems explained. Wiley, New York
Le G, Zhang J (2009) Boundary slip from the immersed boundary lattice Boltzmann models. Phys Rev E 79:026701
Lee T, Lin CL (2005a) Rarefaction and compressibility effects of the lattice-Boltzmann-equation method in a gas microchannel. Phys Rev E 71:046706
Lee T, Lin C-L (2005b) A stable discretization of the lattice Boltzmann equation method for simulation of incompressible two-phase flows at high density ratio. J Comput Phys 206:16–47
Li D (2004) Electrokinetics in microfluidics. Springer
Li H, Fang H (2009) Lattice Boltzmann simulation of electrowetting. Eur Phys J Special Top 171:129–133
Li B, Kwok DY (2003) Lattice Boltzmann model of microfluidics in the presence of external forces. J Colloid Interface Sci 263:144–151
Li B, Kwok DY (2004) Electrokinetic microfluidic phenomena by a lattice Boltzmann model using a modified Poisson-Boltzmann equation with an excluded volume effect. J Chem Phys 120:947–953
Li S, Tafti DK (2007) A mean-field pressure formulation for liquid-vapor flows. J Fluids Eng Trans ASME 129:894–901
Li Q, Wagner AJ (2007) Symmetric free-energy-based multicomponent lattice Boltzmann method. Phys Rev E 76:036701
Li H, Fang H, Lin Z, Xu S, Chen S (2004) Lattice Boltzmann simulation on particle suspensions in a two-dimensional symmetric stenotic artery. Phys Rev E 69:031919
Lim C, Shu C, Niu X, Chew Y (2002) Application of lattice Boltzmann method to simulate microchannel flows. Physics of Fluids 14:2299–2308
Lin Y, Lee C, Lee G (2008) Droplet formation utilizing controllable moving-wall structures for double-emulsion applications. J Microelectromech Syst 17:573–581
Liu C, Ni Y (2008) The effect of surface roughness on rarefied gas flows by lattice Boltzmann method. Chin Phys B 17:4554–4561
Liu H, Zhang Y (2009) Droplet formation in a T-shaped microfluidic junction. J Appl Phys 106:034906
Liu H, Zhou J, Burrows R (2009) Lattice Boltzmann model for shallow water flows in curved and meandering channels. Int J Comput Fluid Dyn 23:209–220

Lobaskin V, Dunweg B, Holm C (2004) Electrophoretic mobility of a charged colloidal particle: a computer simulation study. J Phys Condens Matter 16:S4063–S4073

Luo L (1998) Unified theory of lattice Boltzmann models for nonideal gases. Phys Rev E 81:1618–1621

MacMeccan RM, Clausen JR, Neitzel GP, Aidun CK (2009) Simulating deformable particle suspensions using a coupled lattice-Boltzmann and finite-element method. J Fluid Mech 618:13–39

Madou M, Zoval J, Jia G, Kido H, Kim J, Kim N (2006) Lab on a cd. Ann Rev Biomed Eng 8:601–628

Maier R, Bernard RS (2010) Lattice-Boltzmann accuracy in pore-scale flow simulation. J Comput Phys 229:233–255

Mark D, Metz T, Haeberle S, Lutz S, Ducree J, Zengerle R, von Stetten F (2009) Centrifugo-pneumatic valve for metering of highly wetting liquids on centrifugal microfluidic platforms. Lab Chip 9:3599–3603

Martys NS (2001) Improved approximation of the Brinkman equation using a lattice Boltzmann method. Phys Fluids 13:1807–1810

Martys NS, Chen H (1996) Simulation of multicomponent fluids in complex three-dimensional geometries by the lattice Boltzmann method. Phys Rev E 53:743–750

Masliyah JH, Bhattacharjee S (2006) Electrokinetic and colloid transport phenomena. Wiley

Mei R, Luo L, Lallemand P, d'Humieres D (2006) Consistent initial conditions for lattice Boltzmann simulations. Comput Fluids 35:855–862

Mei R, Luo L-S, Shyy W (1999) An accurate curved boundary treatment in the lattice Boltzmann method. J Stat Phys 155:307–330

Melchionna S, Succi S (2004) Electrorheology in nanopores via lattice Boltzmann simulation. J Chem Phys 120:4492–4497

Meng F, Wang M, Li Z (2008) Lattice Boltzmann simulations of conjugate heat transfer in high-frequency oscillating flows. Int J Heat Fluid Flow 29:1203–1210

Migliorini C, Qian Y, Chen H, Brown E, Jain RK, Munn LL (2002) Red blood cells augment leukocyte rolling in a virtual blood vessel. Biophys J 83:1834–1841

Mo GC, Kwok DY (2006) Multiple separation of self-running drops by pinching a three-phase contact line. Appl Phys Lett 88:064103

Mugele F, Baret JC (2005) Electrowetting: From basics to applications. J Phys Condens Matter 17:R705–R774

Munn LL, Dupin MM (2008) Blood cell interactions and segregation in flow. Ann Biomed Eng 36:534–544

Nie X, Boolen GD, Chen S (2002) Lattice-Boltzmann simulations of fluid flows in MEMS. J Stat Phys 107:279–289

Nijmeijer M, Bruin C, Bakker A, Vanleeuwen J (1990) Wetting and drying of an inert wall by a fluid in a molecular-dynamics simulation. Phys Rev A 42:6052–6059

Nisar A, AftuIpurkar N, Mahaisavariya B, Tuantranont A (2008) MEMS-based micropumps in drug delivery and biomedical applications. Sens Actuators B 130:917–942

Niu X, Shu C, Chew Y (2004) A lattice Boltzmann BGK model for simulation of micro flows. Europhys Lett 67:600–606

Niu X, Shu C, Chew Y, Peng Y (2006) A momentum exchange-based immersed boundary-lattice Boltzmann method for simulating incompressible viscous flows. Phys Lett A 354:173–182

Niu X, Munekata T, Hyodo S, Suga K (2007) An investigation of water-gas transport processes in the gas-diffusion-layer of a PEM fuel cell by a multiphase multiple-relaxation-time lattice Boltzmann model. J Power Sour 172:542–552

Ouared R, Chopard B (2005) Lattice Boltzmann simulations of blood flow: non-Newtonian rheology and clotting processes. J Stat Phys 121:209–221

Pamme N (2006) Magnetism and microfluidics. Lab Chip 6:24–38

Park J, Matsubara M, Li X (2007) Application of lattice Boltzmann method to a micro-scale flow simulation in the porous electrode of a PEM fuel cell. J Power Sour 173:404–414

Pattison MJ, Premnath KN, Morley NB, Abdouc MA (2008) Progress in lattice Boltzmann methods for magnetohydrodynamic flows relevant to fusion applications. Fusion Eng Des 83:557–572

Peng Y, Shu C, Chew Y (2003) A 3D incompressible thermal lattice Boltzmann model and its application to simulate natural convection in a cubic cavity. J Comput Phys 193:260–274

Peskin CS (1977) Numerical analysis of blood flow in the heart. J Comput Phys 25:220–252

Popel AS, Johnson PC (2005) Microcirculation and hemorheology. Ann Rev Fluid Mech 37:43–69

Porter B, Zauel R, Stockman H, Guldberg R, Fyhrie D (2005) 3-D computational modeling of media flow through scaffolds in a perfusion bioreactor. J Biomech 38:543–549

Porter ML, Schaap MG, Wildenschild D (2009) LatticeBoltzmann simulations of the capillary pressuresaturationinterfacial area relationship for porous media. Adv Water Resour 32:1632–1640

Qin RS (2006) Mesoscopic interparticle potentials in the lattice Boltzmann equation for multiphase fluids. Phys Rev E 73: 066703

Qin RS (2007) Bubble formation in lattice Boltzmann immiscible shear flow. J Chem Phys 126:114506

Qian S, Bau H (2009) Magneto-hydrodynamics based microfluidics. Mech Res Commun 36:10–21

Qian Y, d'Humieres D, Lallemand P (1992) Lattice BGK models for Navier-Stokes equation. Europhys Lett 17:479–484

Raabe D (2004) Overview of the lattice Boltzmann method for nano- and microscale fluid dynamics in materials science and engineering. Model Simul Mater Sci Eng 12:R13–R46

Raiskinmaki P, Koponen A, Merikoski J, Timonen J (2000) Spreading dynamics of three-dimensional droplets by the lattice-Boltzmann method. Comput Mater Sci 18:7–12

Raiskinmaki P, Shakib-Manesh A, Jasberg A, Koponen A, Merikoski J, Timonen J (2002) Lattice-Boltzmann simulation of capillary rise dynamics. J Stat Phys 107:143–158

Ramaswamy S, Gupta M, Goel A, Aaltosalmi U, Kataja M, Koponen A, Ramarao BV (2004) The 3D structure of fabric and its relationship to liquid and vapor transport. Colloids Surf A 241:323–333

Reese JM, Zhang Y (2009) Simulating fluid flows in micro and nano devices: the challenge of non-equilibrium behavior. J Comput Theor Nanosci 6:2061–2074

Reis T, Phillips TN (2007) Modified lattice Boltzmann model for axisymmetric flows. Phys Rev E 75:056703

Reneman RS, Arts T, Hoeks APG (2006) Wall shear stress—an important determinant of endothelial cell function and structure—in the arterial system *in vivo*. Vescular Res 43:251–269

Roohi E, Darbandi M, Mirjalili V (2009) Direct simulation monte carlo solution of subsonic flow through micro/nanoscale channels. J Heat Transfer Trans ASME 131:092402

Rowlinson J, Widom B (1982) Molecular theory of capillary. Claredon, Oxford

Sankaranarayanan K, Shan X, Kevrekidis IG, Sundaresan S (1999) Bubble flow simulations with the lattice Boltzmann method. Chem Eng Sci 54:4817–4823

Sbragaglia M, Succi S (2005) Analytical calculation of slip flow in lattice Boltzmann models with kinetic boundary conditions. Phys Fluids 17:093602

Sbragaglia M, Benzi R, Biferale L, Succi S, Toschi F (2006) Surface roughness-hydrophobicity coupling in microchannel and nanochannel flows. Phys Rev Lett 97:204503

Sbragaglia M, Benzi R, Biferale L, Succi S, Sugiyama K, Toschi F (2007) Generalized lattice Boltzmann method with multirange pseudopotential. Phys Rev E 75:026702

Sbragaglia M, Chen H, Shan X, Succi S (2009) Continuum free-energy formulation for a class of lattice Boltzmann multiphase models. EPL 86:24005

Scardovelli R, Zaleski S (1999) Direct numerical simulation of free-surface and interfacial flow. Ann Rev Fluid Mech 31:567–603

Schulz M, Krafczyk M, Tolke J, Rank E (2002) Parallelization strategies and efficiency of CFD computations in complex geometries using lattice Boltzmann methods on high-performance computers. Lect Notes Comput Sci Eng 21:115–122

Sehgal BR, Nourgaliev RR, Dinh TN (1999) Numerical simulation of droplet deformation and break-up by lattice-Boltzmann method. Prog Nuclear Energy 34:471–488

Sethian JA, Smereka P (2003) Level set methods for fluid interfaces. Ann Rev Fluid Mech 35:341–372

Shan X (1997) Simulation of Rayleigh–Benard convection using a lattice Boltzmann method. Phys Rev E 55:2780

Shan X (2008) Pressure tensor calculation in a class of nonideal gas lattice Boltzmann models. Phys Rev E 77:066702

Shan X, Chen H (1993) Lattice Boltzmann model for simulating flows with multiple phases and components. Phys Rev E 47:1815–1819

Shan X, Chen H (1994) Simulation of nonideal gases and liquid-gas phase-transitions by the lattice Boltzmann-equation. Phys Rev E 49:2941–2948

Shan X, Doolen G (1995) Multicomponent lattice-Boltzmann model with interparticle interaction. J Stat Phys 81:379–393

Shan X, Yuan X, Chen H (2006) Kinetic theory representation of hydrodynamics: a way beyond the Navier-Stokes equation. J Fluid Mech 550:413–441

Shi B, Deng B, Du R, Chen X (2008a) A new scheme for source term in LBGK model for convection-diffusion equation. Comput Math Appl 55:1568–1575

Shi Y, Zhao T, Guo Z (2008b) Simplified model and lattice Boltzmann algorithm for microscale electro-osmotic flows and heat transfer. Int J Heat Mass Transf 51:586–596

Sinha PK, Mukherjee PP, Wang C (2007) Impact of GDL structure and wettability on water management in polymer electrolyte fuel cells. J Mater Chem 17:3089–3103

Skordos PA (1993) Initial and boundary-conditions for the lattice Boltzmann method. Phys Rev E 48:4823–4842

Sofonea V, Fruh WG (2001) Lattice Boltzmann model for magnetic fluid interfaces. Eur Phys J B 20:141–149

Sofonea V, Fruh WG, Cristea A (2002) Lattice Boltzmann model for the simulation of interfacial phenomena in magnetic fluids. J Magn Magn Mater 252:144–146

Sofonea V, Sekerka RF (2005) Diffuse-reflection boundary conditions for a thermal lattice Boltzmann model in two dimensions: evidence of temperature jump and slip velocity in microchannels. Phys Rev E 71:066709

Sterling JD, Chen S (1996) Stability analysis of lattice Boltzmann methods. J Comput Phys 123:196–206

Stoltz J, Singh M, Riha P (1999) Hemorheology in practice. IOS Press, Amsterbam

Succi S (2001) The lattice Boltzmann equation. Oxford University Press, Oxford

Succi S (2002) Mesoscopic modeling of slip motion at fluid-solid interfaces with heterogeneous catalysis. Phys Rev Lett 89:064502

Succi S, Vergassola M, Benzi R (1991) Lattice Boltzmann scheme for 2-dimensional magnetohydrodynamics. Phys Rev A 43:4521–4524

Sui Y, Low HT, Chew YT, Roy P (2008) Tank-treading, swinging, and tumbling of liquid-filled elastic capsules in shear flow. Phys Rev E 77:016310

Sukop MC, Thorne DT Jr (2006) Lattice Boltzmann modeling. Springer, Delft

Sullivan DE (1981) Surface tension and contact angle of a liquid-solid interface. J Chem Phys 74:2604–2615

Suzue Y, Shikazono N, Kasagi N (2008) Micro modeling of solid oxide fuel cell anode based on stochastic reconstruction. J Power Sour 184:52–59

Swift MR, Osborn WR, Yeomans JM (1995) Lattice Boltzmann simulation of nonideal fluids. Phys Rev Lett 75:830–833

Swift M, Orlandini E, Osborn W, Yeomans J (1996) Lattice Boltzmann simulations of liquid-gas and binary fluid systems. Phys Rev E 54:5041–5052

Tabe Y, Lee Y, Chikahisa T, Kozakai M (2009) Numerical simulation of liquid water and gas flow in a channel and a simplified gas diffusion layer model of polymer electrolyte membrane fuel cells using the lattice Boltzmann method. J Power Sour 193:24–31

Tang G, Tao W, He Y (2005) Lattice Boltzmann method for gaseous microflows using kinetic theory boundary conditions. Phys Rev E 17:058101

Tang G, Li Z, He Y, Zhao C, Tao W (2007a) Experimental observations and lattice Boltzmann method study of the electroviscous effect for liquid flow in microchannels. J Micromech Microeng 17:539–550

Tang G, Tao W, He Y (2007b) Simulating two- and three-dimensional microflows by the lattice Boltzmann method with kinetic boundary conditions. Int J Modern Phys C 18:805–817

Tang G, Gu X, Barber RW, Emerson DR (2008) Lattice Boltzmann simulation of nonequilibrium effects in oscillatory gas flow. Phys Rev E 78:026706

Teh S, Lin R, Hung L, Lee AP (2008) Droplet microfluidics. Lab Chip 8:198–220

Tian F, Kwok DY (2005) On the surface conductance, flow rate and current continuities of microfluidics with non-uniform surface potentials. Langmuir 21:2192–2198

Tian F, Li B, Kwok DY (2005) Trade-off between mixing and transport for electroosmotic flow in heterogeneous microchannels with nonuniform surface potentials. Langmuir 21:1126–1131

Tolke J, Krafczyk M (2008) TeraFLOP computing on a desktop PC with GPUs for 3D CFD. Int J Comput Fluid Dyn 22:443–456

Tomiyasu J, Inamuro T (2009) Numerical simulations of gas-liquid two-phase flows in a micro porous structure. Eur Phys J Special Top 171:123–127

Toolke J, Freudiger S, Krafczyk M (2006) An adaptive scheme using hierarchical grids for lattice Boltzmann multi-phase flow simulations. Comput Fluids 35:820–830

Tretheway DC, Meinhart CD (2002) Apparent fluid slip at hydrophobic microchannel walls. Phys Fluids 14:L9–L12

Tu J, Yeoh GH, Lin C (2007) Computational fluid dynamics: a practical approach. Butterworth-Heinemann, Oxford

Ubertini S, Succi S (2005) Recent advances of lattice Boltzmann techniques on unstructured grids. Progr Comput Dyn 5:85–96

Upreti SR, Lohi A, Kapadia RA, El-Haj R (2007) Vapor extraction of heavy oil and bitumen:a review. Energy Fuels 21:1562–1574

van der Graaf S, Nisisako T, Schroen C, van der Sman R, Boom R (2006) Lattice Boltzmann simulations of droplet formation in a T-shaped microchannel. Langmuir 22:4144–4152

Verberg R, Pooley CM, Yeomans JM, Balazs AC (2004) Pattern formation in binary fluids confined between rough, chemically heterogeneous surfaces. Phys Rev Lett 93:184501

Verhaeghe F, Luo L, Blanpain B (2009) Lattice Boltzmann modeling of microchannel flow in slip flow regime. J Comput Phys 228:147–157

Voronov RS, Papavassiliou DV, Lee LL (2007) Slip length and contact angle over hydrophobic surfaces. Chem Phys Lett 441:273–276

Wagner AJ, Yeomans JM (1999) Phase separation under shear in two-dimensional binary fluids. Phys Rev E 59:4366–4373

Wang M, Chen S (2007) Electroosmosis in homogeneously charged micro- and nanoscale random porous media. J Colloid Interface Sci 314:264–273
Wang M, Kang Q (2009) Electrokinetic transport in microchannels with random roughness. Anal Chem 81:2953–2961
Wang M, Kang Q (2010a) Modeling electrokinetic flows in microchannels using coupled lattice Boltzmann methods. J Comput Phys 229:728–744
Wang W, Kang Q (2010b) Electrochemomechanical energy conversion efficiency in silica nanochannels. Microfluid Nanofluid. doi: 10.1007/s10404-009-0530-6 (in press)
Wang M, Pan N (2008) Predictions of effective physical properties of complex multiphase materials. Mater Sci Eng R 63:1–30
Wang J, Wang M, Li Z (2005) Lattice Boltzmann simulations of mixing enhancement by the electro-osmotic flow in microchannels. Modern Phys Lett B 19:1515–1518
Wang J, Wang M, Li Z (2006) Lattice Poisson-Boltzmann simulations of electro-osmotic flows in microchannels. J Colloid Interface Sci 296:729–736
Wang J, Wang M, Li Z (2007a) A lattice Boltzmann algorithm for fluid-solid conjugate heat transfer. Int J Therm Sci 46:228–234
Wang M, Pan N, Wang J, Chen S (2007b) Lattice Poisson-Boltzmann simulations of electroosmotic flows in charged anisotropic porous media. Commun Comput Phys 2:1055–1070
Wang M, Wang J, Chen S (2007c) Roughness and cavitations effects on electro-osmotic flows in rough microchannels using the lattice Poisson-Boltzmann methods. J Comput Phys 226:836–851
Warren RB (1997) Electroviscous transport problems via lattice-Boltzmann. Int J Modern Phys C 8:889–898
Weigl BH, Yager P (1999) Microfluidics: microfluidic diffusion-based separation and detection. Science 15:346–347
Widom B (1978) Structure of interfaces from uniformity of the chemical potential. J Stat Phys 19:563–574
Wolf FG, dos Santos LOE, Philippi PC (2009) Modeling and simulation of the fluid–solid interaction in wetting. J Stat Mech Theory Exp. doi:10.1088/1742-5468/2009/06/P06008
Wolf FG, dos Santos LOE, Philippi PC (2010) Capillary rise between parallel plates under dynamic conditions. J Colloid Interface Sci 344:171–179
Wolf-Gladrow DA (2000) Lattice-gas cellular automata and lattice Boltzmann models. Springer, Berlin
Wu H, Huang Y, Wu C, Lee G (2009) Exploitation of a microfluidic device capable of generating size-tunable droplets for gene delivery. Microfluid Nanofluid 7:45–56
Xiong W, Zhang J (2010a) Shear stress variation induced by red blood cell motion in microvessel. Ann Biomed Eng. doi: 10.1007/s10439–010–0017–3 (in press)
Xiong W, Zhang J (2010b) A two-dimensional lattice Boltzmann model for uniform channel flows. Comput Math Appl. doi: 10.1016/j.camwa.2010.02.040 (in press)
Xu K, Li Z (2004) Microchannel flow in the slip regime: gas-kinetic bgk-burnett solutions. J Fluid Mech 513:87–110
Yamaguchi Y, Honda T, Briones MP, Yamashita K, Miyazaki M, Nakamura H, Maeda H (2007) Influence of gravity on two-layer laminar flow in a microchannel. Chem Eng Technol 30:379–382
Yan YY, Zu YQ, Ren LQ, Li JQ (2007) Numerical modelling of electro-osmotically driven flow within the microthin liquid layer near an earthworm surface—a biomimetic approach. Proc Inst Mech Eng C 221:1201–1210
Yang J, Kwok DY (2003) Microfluid flow in circular microchannel with electrokinetic effect and Navier's slip condition. Langmuir 19:1047–1053
Yang AJM, Fleming PD, Gibbs JH (1976) Molecular theory of surface tension. J Chem Phys 64:3732–3747
Yang Z, Dinh TN, Nourgaliev RR, Sehgal BR (2000) Numerical investigation of bubble coalescence characteristics under nucleate boiling condition by a lattice-Boltzmann model. Int J Therm Sci 39:1–17
Yang J, Lu F, Kostiuk LW, Kwok DY (2003) Electrokinetic microchannel battery by means of electrokinetic and microfluidic phenomena. J Micromech Microeng 13:963–970
Yoshino M, Matsuda Y, Shao C (2004) Comparison of accuracy and efficiency between the lattice Boltzmann method and the finite difference method in viscous/thermal fluid flows. Int J Comput Fluid Dyn 18:333–345
Yu D, Mei R, Shyy W (2005) Improved treatment of the open boundary in the method of lattice Boltzmann equation. Progr Comput Fluid Dyn 5:3–12
Yuan P, Schaefer L (2006) Equations of state in a lattice Boltzmann model. Phys Fluids 18:042101
Zagnoni M, Baroud CN, Cooper JM (2009) Electrically initiated upstream coalescence cascade of droplets in a microfluidic flow. Phys Rev E 80:046303
Zeiser T, Bashoor-Zadeh M, Darabi A, Baroud G (2008) Pore-scale analysis of Newtonian flow in the explicit geometry of vertebral trabecular bones using lattice Boltzmann simulation. Proc Inst Mech Eng H 222:185–194
Zhang J, Kwok DY (2004a) Apparent slip over a solid-liquid interface with a no-slip boundary condition. Phys Rev E 70:056701
Zhang J, Kwok DY (2004b) Lattice Boltzmann study on the contact angle and contact line dynamics of liquid-vapor interfaces. Langmuir 20:8137–8141
Zhang J, Kwok DY (2005a) A 2D lattice Boltzmann study on electrohydrodynamic drop deformation with the leaky dielectric theory. J Comput Phys 206:150–161
Zhang J, Kwok DY (2005b) On the validity of the Cassie equation via a mean-field free-energy lattice Boltzmannapproach. J Colloid Interface Sci 282:434–438
Zhang J, Kwok DY (2006a) Contact line and contact angle dynamics in superhydrophobic channels. Langmuir 22:4998–5004
Zhang J, Kwok DY (2006b) Pressure boundary condition of the lattice Boltzmann method for fully developed periodic flows. Phys Rev E 73:047702
Zhang J, Kwok DY (2009) A mean-field free energy lattice Boltzmann model for multicomponent fluids. Eur Phys J Special Top 171:45–53
Zhang J, Kwok DY (2010) Roughness effects on continuous and discrete flows in superhydrophobic microchannels. Commun Comput Phys (submitted)
Zhang J, Tian F (2008) A bottom-up approach to non-ideal fluids in the lattice Boltzmann method. Europhys Lett 81:66005
Zhang J, Li B, Kwok DY (2004) Mean-field free-energy approach to the lattice Boltzmann method for liquid-vapor and solid-fluid interfaces. Phys Rev E 69:032602
Zhang Y, Qin R, Emerson DR (2005a) Lattice Boltzmann simulation of rarefied gas flows in microchannels. Phys Rev E 71:047702
Zhang Y, Qin R, Sun Y, Barber RW, Emerson DR (2005b) Gas flow in microchannels—a lattice Boltzmann method approach. J Stat Phys 121:257–267
Zhang R, Shan X, Chen H (2006) Efficient kinetic method for fluid simulation beyond the Navier-Stokes equation. Phys Rev E 74:046703
Zhang J, Johnson PC, Popel AS (2007) An immersed boundary lattice Boltzmann approach to simulate deformable liquid capsules and its application to microscopic blood flows. Phys Biol 4:285–295
Zhang J, Johnson PC, Popel AS (2008) Red blood cell aggregation and dissociation in shear flows simulated by lattice Boltzmann method. J Biomech 41:47–55
Zhang J, Johnson PC, Popel AS (2009a) Effects of erythrocyte deformability and aggregation on the cell free layer and apparent viscosity of microscopic blood flows. Microvasc Res 77:265–272

Zhang J, Li B, Kwok DY (2009b) Metastable contact angles and self-propelled drop movement on chemically heterogeneous surfaces by a mean-field lattice Boltzmann model. Eur Phys J Special Top 171:73–79

Zhang J, Liu Y, Zhang J, Yang J (2009c) Study of force-dependent and time-dependent transition of secondary flow in a rotating straight channel by the lattice Boltzmann method. Phys A 388:288–294

Zhang J, Johnson PC, Popel AS (2010) Simulating microscopic hemodynamics and hemorheology with the immersed-boundary lattice-Boltzmann method. In: Pozrikidis C (ed) Computational hydrodynamics of capsules and biological cells. CRC, Boca Raton

Zheng HW, Shu C, Chew YT (2006) A lattice Boltzmann model for multiphase flows with large density ratio. J Comput Phys 218:353–371

Zhu Y, Granick S (2002) Limits of the hydrodynamic no-slip boundary condition. Phys Rev Lett 88:106102

Zhu L, Tretheway D, Petzold L, Meinhart C (2005) Simulation of fluid slip at 3D hydrophobic microchannel walls by the lattice Boltzmann method. J Comput Phys 202:181–195

Zou Q, He X (1997) On pressure and velocity boundary conditions for the lattice Boltzmann BGK model. Phys Fluids 9:1591